

MODELING THE OCEANIC LITHOSPHERE OBDUCTION: CONSTRAINTS FROM THE METAMORPHIC SOLE OF MIRDITA OPHIOLITES (NORTHERN ALBANIA)

Laura Gaggero*, Michele Marroni**✉, Luca Pandolfi** and Laura Buzzi*

* Dipartimento per lo Studio del Territorio e delle sue Risorse, Università di Genova, Italy.

** Dipartimento di Scienze della Terra, Università di Pisa and CNR, Istituto di Geoscienze e Georisorse, Sezione di Pisa, Italy.

✉ Corresponding author, e-mail: marroni@dst.unipi.it

Keywords: *Intra-oceanic thrusting, metamorphic sole, marginal stage, obduction, OIB, WPB, geochemistry, geothermobarometry. Mirdita, northern Albania.*

ABSTRACT

The Hellenic-Dinaric belt of the Eastern Mediterranean sea is characterized by huge and well preserved obducted slices of ophiolites. A well developed and very thick metamorphic sole generally occurs at the base of the obducted ophiolite sequences. The best preserved metamorphic sole of the Hellenic-Dinaric belt crops out in association with the Albanian ophiolites. In the Mirdita area (northern Albania) the metamorphic sole consists of an up to 600 m thick assemblage of metasediments and amphibolites. Four different types of amphibolites, referred as T1 to T4, have been identified on the basis of grain-size and mineralogical assemblages. The protoliths of all the amphibolites are basic rocks with OIB affinity, representative of within-plate magmatism typical of oceanic seamounts; no MORB derived rocks have been identified. The associated metasedimentary rocks are presumably derived from oceanic covers. All the lithologies from the Mirdita metamorphic sole are strongly deformed under lower to upper amphibolite facies conditions. A discontinuous inverted gradient is observed close to harzburgites in the metamorphic sole, that shows high-grade amphibolite facies metamorphism. There are no prograde greenschist facies metamorphic rocks, although all the lithologies from the Mirdita metamorphic sole are affected by greenschist facies retrogression. The different types of amphibolites display different P and T values at metamorphic climax conditions. The temperatures range from $624\pm 9^\circ$ to $796\pm 50^\circ\text{C}$ in the different units where the pressure is always lower than 0.7 GPa. The boundaries between the amphibolite slices with different peak metamorphism as well as the bodies of the gneisses and micaschists are sheared bands. The structural pattern common to all lithologies identified in the Mirdita metamorphic sole developed through two deformation phases under amphibolite facies conditions, followed by a third phase under greenschist facies. The petrologic and structural characteristics of the metamorphic sole are discussed in order to highlight the kinematics of the obduction process.

INTRODUCTION

Ophiolitic sequences along the main suture zones of collisional belts are considered as remnants of oceanic lithosphere. These ophiolites can occur in different occurrences: I) folded metaophiolite sequences, affected by high pressure metamorphism followed by decompression recrystallization, which are interpreted as fragments of oceanic lithosphere involved in subduction-related processes (e.g., Kurz and Froitzheim, 2002; Miller and Cartwright, 2000), II) ophiolitic slices, implicated in flysch sequences and generally affected by a very low-temperature metamorphic overprint, likely emplaced at shallow levels in accretionary prisms (e.g., Cloos and Shreve, 1988; Meneghini et al., 2009), III) ophiolitic sequences overlying the continental lithosphere and lacking penetrative deformation and metamorphism, which are considered as emplaced by obduction (e.g., Stampfli et al., 1998; Wemjiao et al., 2002).

Several key examples of obducted ophiolitic sequences occur in the Tethyan collisional belts of the Eastern Mediterranean (Coleman, 1981; Lytwyn and Casey 1995; Carosi et al., 1996). The obducted ophiolitic sequences typically include thick slices of undeformed oceanic lithosphere that originated in a supra-subduction zone, detached from their mantle basement and emplaced over adjacent continental margins (Spray, 1983). According to Michard et al. (1991), their emplacement included an early, intra-oceanic stage of thrusting characterized by the development of a metamorphic sole. The intra-oceanic stage was followed by a marginal stage with the oceanic lithosphere overriding the continental

margin (Gray and Gregory, 2000; Bortolotti et al., 2005).

However, some features of the obduction process are still a matter for debate. For example, the site of intra-oceanic detachment, the nature of the involved oceanic crust and the depth of the metamorphic processes (i.e. the geometry of the intraoceanic thrust surfaces) are still unclear. Valuable insights into the obduction process can be gained from petrologic and structural analysis of the metamorphic sole.

Within the Hellenic Dinaric orogenic belt of the Eastern Mediterranean, a well-developed and very thick metamorphic sole occurs at the base of the Albanian ophiolites (Carosi et al., 1996; Dimo-Lahitte et al., 2001). This paper presents a study of the metamorphic sole below the Northern Albanian ophiolites aimed to identify 1) the nature and origin of its igneous protoliths, 2) the structural setting at meso- and microscale and 3) the metamorphic evolution, in order to provide useful constraints for the reconstruction of the kinematics of the metamorphic sole and its geodynamic setting.

REGIONAL GEOLOGY

In the Hellenic-Dinaric orogenic belt, large ophiolitic nappes overlie the continental margin sequences. The ophiolites are regarded as slices of the Mesozoic Tethyan oceanic lithosphere obducted onto the continental margin(s) during the Late Jurassic convergence, which has related to the north-eastward translation of Adria toward the Eurasia plate (e.g., Robertson and Dixon, 1984).

The Mirdita ophiolites in northern Albania (Figure 1) rep-

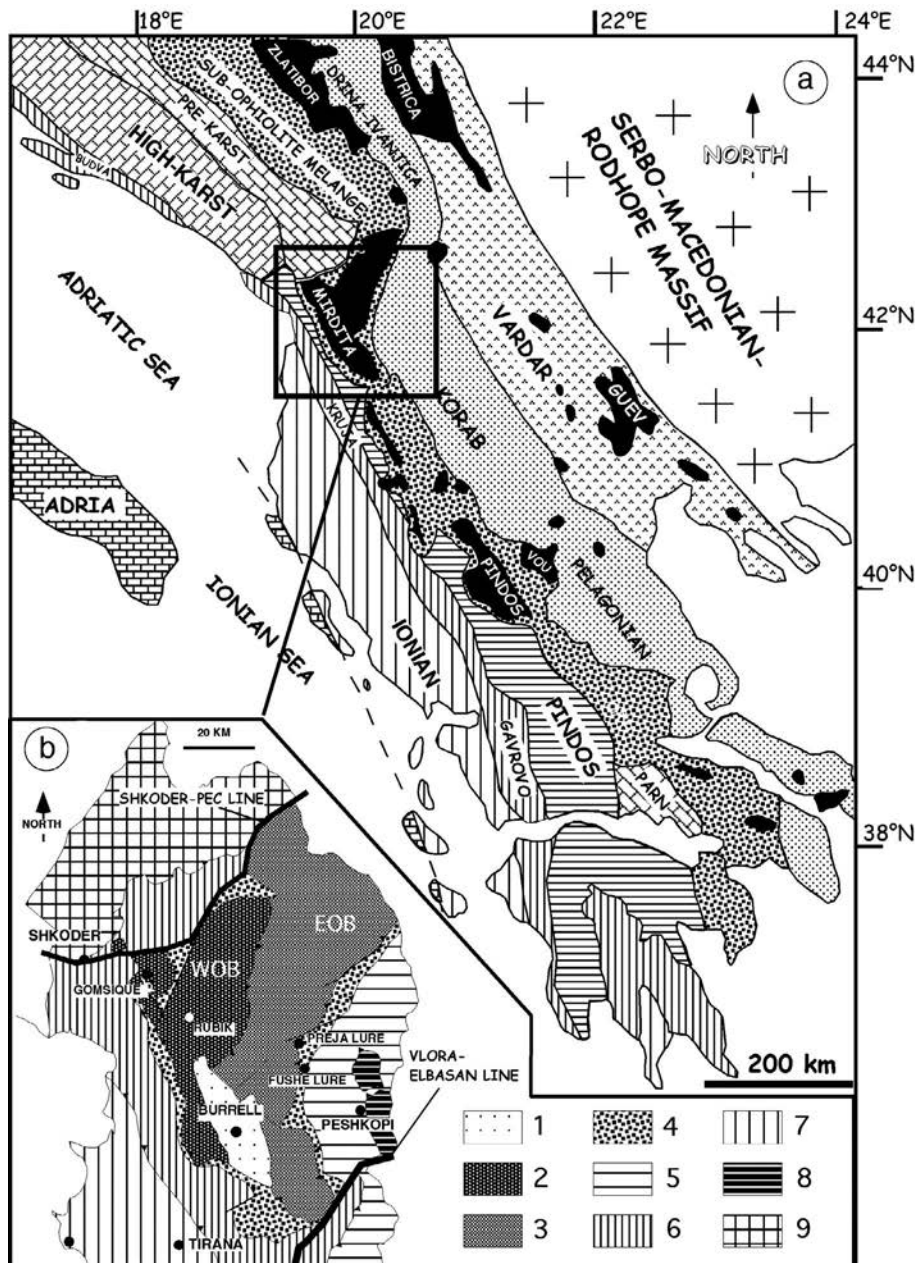


Fig. 1 - a) Tectonic scheme and location of the major ophiolitic massifs (solid black) in the Dinaric-Hellenic belt, modified after Aubouin et al. (1970). Abbreviations: Guev = Guevgueli; Vou = Vourinos; Oth = Othris; Parn = Parnassus Zone. Box indicates the investigated area. b) Tectonic sketch of the Mirdita area, northern (Albania). Abbreviation: 1. Late Tertiary molasse deposits; 2. Western belt ophiolite sequence (WOB); 3. Eastern belt ophiolite sequence (EOB); 4. Rubik melange; 5. Pelagonian units; 6. Krastaçuali unit; 7. Kruja unit; 8. Units of the Peshkopi window; 9. Albanian Alps.

represent one of the largest and best preserved oceanic fragments cropping out the Hellenic-Dinaric orogenic belt (Çollaku et al., 1991; Beccaluva et al., 1994; Shallo, 1994; Kodra et al., 2000; Robertson and Shallo, 2000; Bortolotti et al., 2002; 2004; Hoeck et al., 2002; Saccani et al., 2004, 2008a; 2008b; Dilek et al., 2005; 2007; 2008). The ophiolites are subdivided into two different sequences, known as the western and eastern ophiolitic belt, hereafter respectively referred to as WOB and EOB (Shallo et al., 1987; Shallo, 1994; Beccaluva et al., 1994), both belonging to the same oceanic basin (Bortolotti et al., 1996; 2004; Bébien et al., 1998; 2000; Inserguex-Filippi et al., 2000; Saccani et al., 2008a; 2008b).

The WOB shows a sequence about 3-4 km thick that mainly includes, from bottom up: lherzolitic mantle tectonites, a gabbroic intrusive sequence, a discontinuous sheeted dike complex and pillow-lava basalts with high-Ti (MORB) affinity (Beccaluva et al., 1994). The WOB represents a MOR-type ophiolite that probably developed in a low- or intermediate-spreading rate ridge (Cortesogno et al., 1998; Nicolas et al., 1999). However, also volcanic se-

quences with intermediate MORB-IAT geochemical features and very low-Ti basalt dikes are found in the WOB (Bortolotti et al., 1996).

The EOB, up to 10 km thick, includes an oceanic sequence consisting of mantle harzburgites, mafic-ultramafic cumulates, a well developed sheeted dike complex and a volcanic sequence of massive and pillow basalts, basalt andesites, andesites, dacites and rhyolites (e.g., Shallo, 1994). Boninitic dikes have also been reported by Beccaluva et al. (1994). In the EOB, the IAT geochemical characterization of the basalt rocks supports an origin in a supra-subduction basin (Beccaluva et al., 1994; Shallo, 1994; Saccani et al., 2004; Dilek et al., 2005; 2007; 2008).

The WOB is representative of a MOR oceanic lithosphere but the occurrence of IAT basalts indicates that the oceanic basin from which these ophiolites derived had experienced a two-stage crustal growth (Bortolotti et al., 1996; 2002). In the first stage, MOR-type oceanic lithosphere was generated at a mid-ocean ridge spreading center. Subsequently, during the second stage, a portion of this lithos-

phere was trapped in the supra-subduction setting (most probably in a proto-forearc region) with consequent generation of IAT basalts. So, the western ophiolites can be interpreted as a MOR oceanic lithosphere trapped over a subduction zone (Bortolotti et al., 2002; 2004). In turn, the eastern ophiolites represent an oceanic lithosphere entirely developed in a suprasubduction zone (Beccaluva et al., 1994; Saccani et al., 2004; Dilek et al., 2005; 2007; 2008).

In both the WOB and EOB the sedimentary cover of ophiolites consists of radiolarites (Kalur Cherts), ranging in age from late Bathonian/early Callovian to middle Callovian/early Oxfordian (Marcucci and Prela, 1996). The similar age of the overlying sediments (Marcucci and Prela, 1996) indicates that the IAT basalts in the eastern and western units have the same age and originated in the same oceanic environment during the Middle Jurassic. This oceanic basin, located over a subduction zone, was therefore characterized by a trapped MOR lithosphere where a younger oceanic lithosphere, originating entirely in a supra-subduction zone, probably in a fore-arc setting, was being formed.

Well developed metamorphic soles have been recognized at the base of both the WOB and EOB sequences (Çollaku et al., 1992; Hoxha et al., 1993; Carosi et al., 1996; Dimo-Lahitte et al., 2001). In the Mirdita region, the WOB and EOB sequences overlie the Rubik Complex (Bortolotti et al., 2005), which consists of an assemblage of thrust slices derived from both the continental and oceanic domains. The slices of continental origin generally consist of Triassic to Jurassic carbonate successions. In addition, slices consisting of within-plate to transitional igneous rocks emplaced in a continental setting during the Anisian have also been recognized. However, the most widespread igneous rocks, found as a slice at the top of the Rubik Complex, are represented by an up to 500 m thick sequence of MOR pillow-lava basalts alternating with Middle to Late Triassic radiolarites (Bortolotti et al., 2004; 2005), known as the "Volcano-sedimentary Formation" or Porava Unit (Bortolotti et al., 2006). In the Rubik Complex, other oceanic-derived slices are mainly represented by serpentinites. The history of the Rubik Complex, better recorded in the "Volcano-sedimentary Formation" includes two superimposed folding phases, both developed under sub-greenschist facies metamorphic conditions (Carosi et al., 1996).

Both ophiolitic belts are unconformably covered by a sedimentary succession including the late Tithonian - Valanginian Simoni Mélange and Firza Flysch (Bortolotti et al., 1996; Chiari et al., 2008), in turn unconformably topped by Barremian-Senonian shallow-water carbonate deposits (Bortolotti et al., 1996; Chiari et al., 2007; Gawlick et al., 2008).

GEOLOGICAL SETTING OF THE ALBANIAN METAMORPHIC SOLE

The metamorphic sole below the WOB was investigated along two SW to NE geotraverses: 1) between the villages of Rubiku and Rresheni, 2) west of Lake Shkoder. No differences in the lithologies of the metamorphic soles below the EOB and WOB was detected.

The metamorphic sole is generally sandwiched between the peridotites of the ophiolitic sequence and the Rubik Complex. The boundary with the underlying Rubik Complex is represented by a low-angle, cataclastic shear zone, characterized by a top-to-west shear sense (Figure 2). The basal part of the peridotites exhibits obduction-related, low-temperature

mylonitic deformation (e.g., Hoxha and Boullier, 1995).

The metamorphic sole in both EOB and WOB consists of alternating banded garnet-bearing gneisses, micaceous-quartz-schists (hereafter referred to as micaschists), fine-grained amphibolites, coarse-grained augen amphibolites, and fine- to medium-grained, sometimes garnet-bearing, amphibolites (Table 1). The metamorphic sole has a wide thickness range, from 5-10 meters up to more than 500 meters, mainly resulting from Tertiary brittle deformation that produced a strong boudinage during thrust tectonics. The maximum thickness is attained in the EOB, near the village of Preja Lure (Figure 1), where the metamorphic sole is about 600 m thick.

Four types of amphibolites have been identified, and referred to as T1 to T4 types, showing differences in grain size and mineralogical assemblage (Carosi et al., 1996). T1 to T4 types of amphibolites show the same composition and metamorphic features in both WOB and EOB. This evidence suggests that the WOB and EOB represent the same continuous structural level at the base of the peridotites.

The T1 amphibolites generally show homogeneous composition and prevail in the outcrops. They occur as decimetre to hundreds of meter-thick lenses or boudins interbedded within the micaschists. T2 amphibolites generally are identified as thickest lens-shaped slices. The T1 and T2 amphibolites generally occur at the base of the metamorphic sole. The T3 garnet-bearing amphibolites are recognized as decimetre-thick lenses associated with garnet-bearing gneisses. T4 amphibolites occurs interbedded with garnet-bearing gneisses and often also with T3 amphibolites. The T3 and T4 amphibolites occur close to the overlying peridotites.

The amphibolites show different field and frequency occurrence in the WOB and EOB. In the WOB, T1 amphibolites are more abundant and T2 are relatively widespread, whereas T4 are rare. In the EOB, T3 amphibolites are prevalent and T4 relatively frequent. The garnet-gneisses attain their maximum thickness in the EOB. In the EOB the retrograde overprint is widespread, and rodingitization along mylonitic contacts between metabasites and serpentinites is frequent. In the WOB, the retrograde processes are localized along thin shear bands.

The WOB and EOB metamorphic soles are characterized by a main, composite schistosity, referred as S_1 - S_2 foliation, that is found everywhere parallel to the contact between the harzburgites and the Rubik complex. The S_1 - S_2 schistosity, developed during metamorphic peak conditions within amphibolite facies, bears well-developed mineral lineations consisting of oriented amphiboles and/or plagioclases lying on the main foliation. Mineral lineations (Figure 2) show WNW-ESE to NWSE strikes in the WOB (Carosi et al., 1996), whereas they display NWSE strikes in the EOB (Çollaku et al., 1992; Carosi et al., 1996).

The kinematic indicators from the WOB metamorphic sole clearly reveal a top-to-the west sense of shear (Carosi et al. 1996). The same structural elements in the eastern metamorphic sole provide contrasting kinematics. According to Çollaku et al. (1991), Carosi et al. (1996) and Bortolotti et al. (2005) the sense of shear is top-to-the-west, whereas Dimo-Lahitte et al. (2001) indicate coexistence of top-to-the west and top-to-the-east indicators, with the latter prevailing.

Mylonitic to cataclastic shear zones are sometimes recognized at the boundaries of the different lithologic units identified in the metamorphic sole. A retrograde phase, identified in both WOB and EOB, is represented by folds and a crenulation cleavage, referred as S_3 foliation, under green-

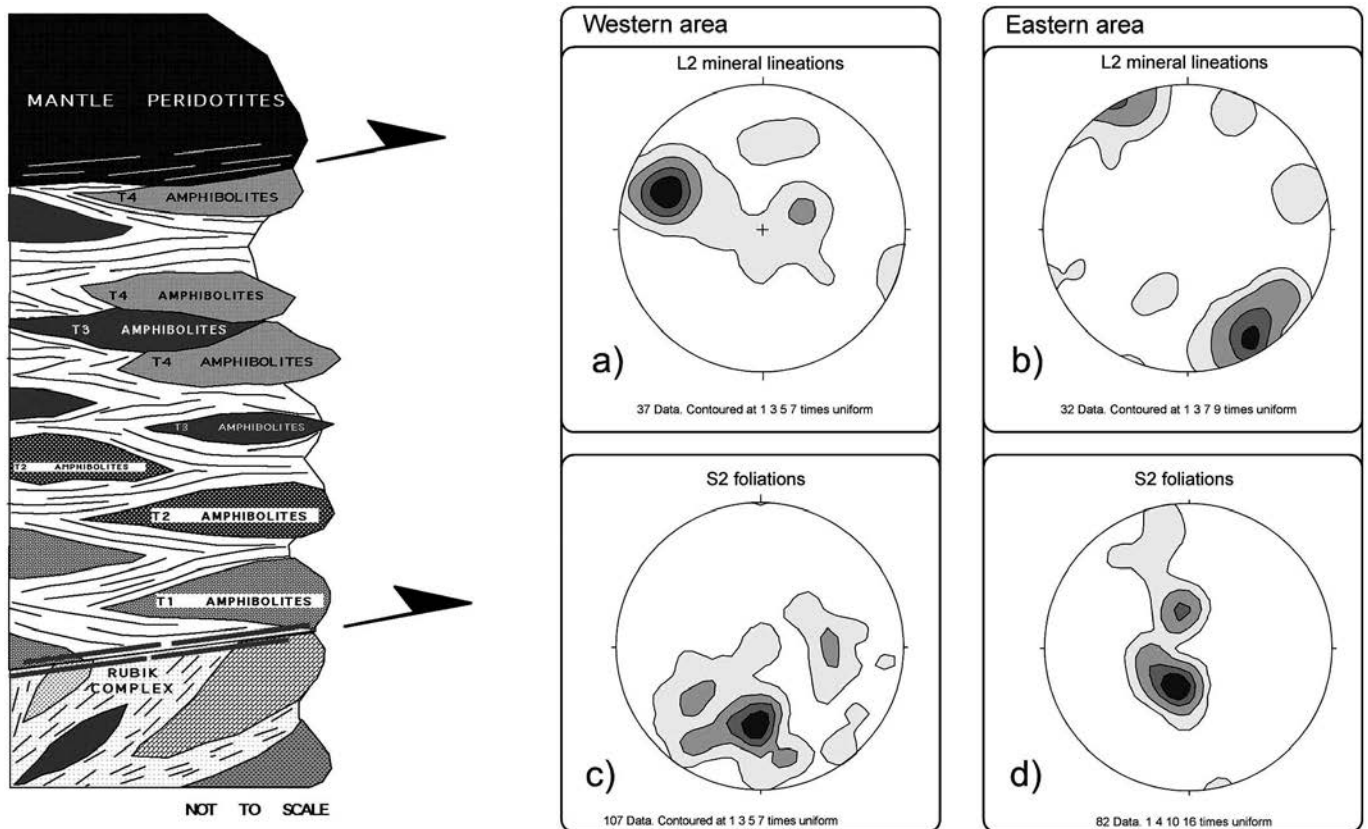


Fig. 2 - Reconstructed stratigraphy of the metamorphic sole from Mirdita ophiolitic nappe not to scale on the basis of all the data collected from the WOB and EOB and stereoplots related to L1/L2 and S1/S2 structural elements. a) and b) L2 mineral lineation; c) and d) S2 foliation (Schmidt net, lower hemisphere, modified after Bortolotti et al., 2005).

schist facies conditions (Carosi et al., 1996). Subsequently, both the metamorphic sole and the Rubik complex were folded together by a D_4 phase characterized by west-verging, asymmetric folds with NE/SW striking axes.

The metamorphic sole is roughly coeval with the age of the radiolarites, and ranges from 162.4 ± 2.4 Ma to 172.6 ± 1.7 Ma, as determined by ^{40}Ar - ^{39}Ar systematics on amphiboles and white micas (Vergely et al., 1998). No differences in the age determinations were detected between the WOB and EOB soles.

PROTOLITHS AND PETROGENETIC SETTINGS.

Petrographic features

The mesoscale features of metamorphic sole lithologies reflect their macroscopic field features. All the amphibolite types and the metasedimentary rocks from the metamorphic sole were investigated both at the meso- and microscale.

The T1 amphibolites consist of fine-grained, clinozoisite and plagioclase-bearing rocks with pervasive, composite S_1 - S_2 schistosity (Figure 3a). Hinges of intrafoliar folds, often boudinaged, have preserved S_1 textural relics. The relic mineral grains are rotated and coarser (0.5-0.6 mm) than the isoriented syn-kinematic grains along S_2 (0.1-0.5 mm). The mineral assemblage in the S_1 - S_2 schistosity is represented by brown-green hornblende (60-65% in volume), + plagioclase (20-23% in volume), + clinozoisite (12-15% in volume), + accessory ilmenite \pm rutile \pm quartz \pm muscovite \pm apatite. A greenschist facies overprint (actinolite + albite + epidote + chlorite + titanite) is widespread and associated with the S_3 event.

The medium- to coarse-grained augen amphibolites belong to T2. The T2 amphibolites have an average grain size in the range 0.2-3.0 mm (Figure 3b). Green to brown-green hornblende (30-95% in volume) coexists with plagioclase (5-55%), clinopyroxene (0-15%) and clinozoisite (0-10%). Rutile is restricted to plagioclase-poor compositions; titanite, sometimes with rutile cores, is more diffuse as inclusions in hornblende, whereas ilmenite occurs rarely. The S_1 foliation preserved in lens-shaped centimetre to decimetre-thick domains shows a broad compositional banding, and is characterized by large (> 2.0 mm) poikiloblastic hornblende and clinopyroxene including smaller hornblende and plagioclase grains. Euhedral inclusions of plagioclase within clinopyroxene represent relic igneous (ophitic) textures. The S_2 schistosity is characterized by grain-size reduction and rotation and by development of nematoblastic to decussate clinopyroxene, granoblastic plagioclase and clinozoisite, without significant changes in mineral composition. A spaced S_3 cleavage is associated with folding and with retrograde greenschist facies alteration (epidote, albite, actinolite). Later fractures were filled by epidote, prehnite, chlorite, and tremolite.

T3 consists of medium-grained, brown hornblende and garnet-bearing amphibolites (Figure 3c). The mineral composition is represented by reddish to brown hornblende (30-50%), plagioclase (20-40%) \pm clinopyroxene (0-25%) \pm garnet (0-10%) \pm quartz (0-5%). Titanite is diffuse, commonly overgrowing rutile and ilmenite. Relics of the S_1 foliation are mostly preserved as inclusions in garnet (hornblende, plagioclase, clinopyroxene, biotite, quartz and rutile). S_2 is characterized by rotation, re-orientation and grain reduction and by syn-kinematic recrystallization. A greenschist facies

Table 1 - Localization of samples.

| Sample | Locality | Latitude | Longitude | Altitude (m) |
|--------|-------------|---------------|---------------|--------------|
| GL 03 | Fushe-Lura | 41°47'22.51"N | 20°14'00.31"E | 1251 |
| GL 04 | Fushe-Lura | 41°47'20.62"N | 20°13'57.71"E | 1261 |
| GL 08 | Fushe-Lura | 41°47'17.51"N | 20°13'54.85"E | 1246 |
| GL 12 | Fushe-Lura | 41°47'14.52"N | 20°13'56.99"E | 1275 |
| GL 13 | Fushe-Lura | 41°47'11.84"N | 20°13'53.67"E | 1254 |
| GL 14 | Fushe-Lura | 41°47'08.66"N | 20°13'55.55"E | 1273 |
| GL 15 | Fushe-Lura | 41°47'05.07"N | 20°13'52.25"E | 1276 |
| GL 17 | Fushe-Lura | 41°49'49.90"N | 20°13'50.18"E | 1275 |
| GL 22 | Pregje-Lura | 41°47'00.39"N | 20°13'08.02"E | 1088 |
| GL 28 | Pregje-Lura | 41°47'50.76"N | 20°13'05.04"E | 1074 |
| GL 32 | Pregje-Lura | 41°50'00.21"N | 20°13'12.27"E | 1077 |
| GL 35 | Pregje-Lura | 41°50'00.96"N | 20°13'10.56"E | 1066 |
| SQ 02 | Gomsique | 42°00'33.83"N | 19°40'16.20"E | 240 |
| SQ 03 | Gomsique | 42°00'33.62"N | 19°40'16.95"E | 244 |
| SQ 04 | Gomsique | 42°00'33.20"N | 19°40'17.67"E | 246 |
| SQ 08 | Gomsique | 42°00'33.10"N | 19°40'17.75"E | 249 |
| SQ 09 | Gomsique | 41°58'56.20"N | 19°47'27.91"E | 350 |
| SQ 18 | Rubik | 41°47'35.55"N | 19°48'37.63"E | 151 |
| SQ 20 | Rubik | 41°48'13.41"N | 19°48'04.25"E | 270 |
| SQ 25 | Rubik | 41°48'11.49"N | 19°48'04.84"E | 260 |
| SQ 26 | Gomsique | 42°00'36.97"N | 19°39'19.80"E | 123 |
| SQ 35 | Gomsique | 42°00'32.56"N | 19°40'20.17"E | 258 |
| SQ 36 | Gomsique | 41°58'58.24"N | 19°47'30.47"E | 348 |
| SQ 38 | Gomsique | 41°58'58.38"N | 19°47'30.95"E | 349 |
| SQ 40 | Gomsique | 41°58'58.68"N | 19°47'31.69"E | 350 |
| SQ 42 | Gomsique | 41°58'58.82"N | 19°47'32.18"E | 351 |
| SQ 44 | Gomsique | 41°58'58.85"N | 19°47'32.22"E | 352 |
| SQ 45 | Gomsique | 41°58'58.90"N | 19°47'32.29"E | 352 |
| SQ 47 | Gomsique | 41°58'59.00"N | 19°47'32.37"E | 352 |
| SQ 48 | Gomsique | 41°58'59.10"N | 19°47'32.39"E | 352 |
| SQ 49 | Gomsique | 41°58'59.10"N | 19°47'32.41"E | 352 |
| SQ 50 | Gomsique | 41°58'59.80"N | 19°47'32.49"E | 353 |
| SQ 52 | Gomsique | 41°58'22.64"N | 19°43'54.52"E | 230 |
| SQ 55 | Gomsique | 41°58'22.07"N | 19°43'55.17"E | 224 |
| SQ 56 | Gomsique | 41°58'22.04"N | 19°43'55.53"E | 223 |
| SQ 57 | Gomsique | 41°58'21.72"N | 19°43'56.57"E | 217 |
| SQ 60 | Gomsique | 41°58'21.66"N | 19°43'57.29"E | 215 |
| SQ 61 | Gomsique | 41°58'21.64"N | 19°43'57.65"E | 213 |
| SQ 64 | Gomsique | 41°58'22.09"N | 19°43'57.76"E | 219 |
| SQ 65 | Gomsique | 41°58'21.53"N | 19°43'59.04"E | 223 |
| SQ 66 | Gomsique | 41°58'21.21"N | 19°43'59.70"E | 228 |
| SQ 67 | Gomsique | 41°58'59.24"N | 19°47'33.63"E | 353 |
| SQ 68 | Gomsique | 41°58'59.33"N | 19°47'33.69"E | 354 |
| SQ 80 | Fushe-Lura | 41°47'10.20"N | 20°14'01.40"E | 1365 |
| SQ 81 | Fushe-Lura | 41°47'10.33"N | 20°14'01.49"E | 1365 |
| SQ 82 | Fushe-Lura | 41°47'10.42"N | 20°14'01.55"E | 1366 |
| SQ 83 | Fushe-Lura | 41°47'10.59"N | 20°14'01.44"E | 1366 |
| SQ 86 | Fushe-Lura | 41°47'10.64"N | 20°14'01.38"E | 1364 |
| SQ 92 | Fushe-Lura | 41°47'07.80"N | 20°14'00.95"E | 1371 |
| SQ 93 | Fushe-Lura | 41°47'07.95"N | 20°14'00.88"E | 1368 |
| SQ 95 | Fushe-Lura | 41°47'08.01"N | 20°14'00.75"E | 1366 |
| SQ 96 | Fushe-Lura | 41°47'08.00"N | 20°14'00.80"E | 1366 |
| SQ 101 | Fushe-Lura | 41°47'05.10"N | 20°13'53.62"E | 1294 |
| SQ 102 | Fushe-Lura | 41°47'04.46"N | 20°13'52.60"E | 1283 |
| SQ 103 | Fushe-Lura | 41°47'03.81"N | 20°13'51.57"E | 1273 |

Series GL: Eastern metamorphic sole (present work); Series SQ: Western metamorphic sole (Carosi et al., 1996).

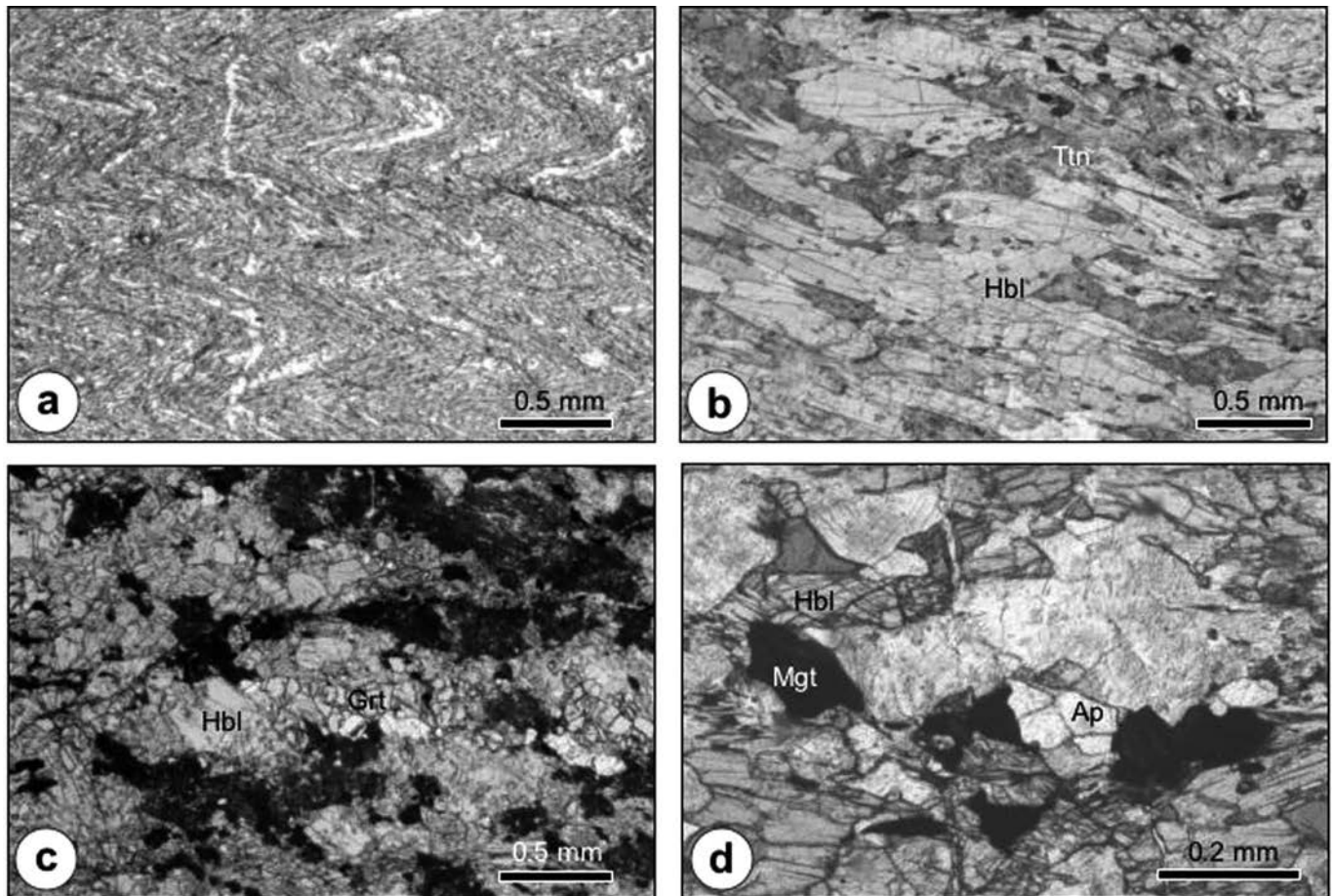


Fig. 3 - Amphibolite type mineralogy and fabric. a) Type 1 metabasalt: S₁ schistosity, crenulated by S₂, defined by plagioclase and amphibole; b) Type 2 metaintrusive rock: hornblende, plagioclase, titanite aligned on S₁; c) Type 3 metaintrusive rock: polyphase garnet and hornblende; d) Type 4 metaintrusive rock: Fe- and Fe-Ti oxide, apatite, hornblende assemblage recording cumulus texture.

overprint is poorly developed. Later prehnite-bearing assemblages are also recognized in fractures.

T4 includes fine- to medium-grained amphibolites, generally ilmenite- and apatite-rich (Figure 3d). The grain-size of T4 amphibolites varies between 0.1 and 0.4 mm. The modal composition includes amphibole ($\approx 48\%$) and plagioclase ($\approx 37\%$). The occurrence of K-feldspar (5-7%), and/or biotite (3-4%), greenish clinopyroxene ($\approx 3\%$), and relatively abundant ilmenite and apatite is a distinctive feature. Quartz is rare and titanite occurs diffusely. The retrograde overprint is poorly developed.

The metasedimentary rocks are mainly gneisses and micaschists. In the gneisses, the S₁-S₂ composite schistosity results in sub-millimetric quartz and mica layers. Quartz is predominant (30-40%), with variable but abundant muscovite, garnet, plagioclase, biotite, and minor clinzoisite, apatite, rutile, magnetite and tourmaline lying on the main schistosity. Lens-shaped aggregates of relatively large isoriented micas, garnet and plagioclase, wrapped in lepidoblastic micas, are relics of the D₁ event. The garnet is commonly zoned and includes biotite, muscovite and quartz, sometimes as snowball textures. The micaschists are characterized by a planar S₁-S₂ composite schistosity; a centimeter to meter thick compositional banding parallel to the schistosity is the dominant feature. Quartz is the main constituent, with muscovite (10-40%), and subordinate biotite (0-10%).

Chemical characterization

Ocean-derived rocks identified in the metamorphic sole as well as continental lithologies were densely sampled in order to identify their protoliths. Whole rock major and trace element abundances for the amphibolites and for the metasediments were carried out by XRF techniques at X-RAL Laboratories, Canada. Losses on ignition (LOI) were determined by the gravimetric method. The RE elements were analyzed by ICP-MS at X-RAL Laboratories, Canada. Detection limits are reported in Tables 2 and 3.

T1 amphibolites have a homogeneous composition, corresponding to basalts in the TAS diagram (not reported) and to subalkalic andesite basalt, based on less mobile elements (Figure 4). Relatively evolved compositions are also consistent with Mg# in the range 31.49-55.46. TiO₂, Zr and Y inversely correlate with Mg#, whereas P₂O₅ has a relatively flat trend (Fig. 5). The REE patterns (Fig. 6) are relatively flat (LaN/YbN = 0.49-8.98) with HREE about 10-20 chondrite (Σ HREE: 4.32-12.05; GdN/YbN = 0.94-1.68) and slightly depleted LREE (Σ LREE: 25.00-106.60; LaN/SmN = 0.43-3.79).

T2 amphibolites show a large compositional range with SiO₂ between 45.1 and 49.4 wt%, relatively low Fe₂O₃ (4.1-11.3 wt%) and high MgO (6.4-24.0 wt%), (Figure 5). Different Mg# intervals (64.6-77.6 and 40.2-62.9) allow to distinguish 1) a group with REE depleted patterns (Σ REE: 3.76-11.44 ppm; Σ HREE=0.84-2.10 ppm), low LREE

Table 2 - Major and trace element compositions of Eastern (present work) and Western (Carosi et al., 1996) amphibolites.

| Type Sample | T1 GL17 Gure Lura village | T1 GL4 Gure Lura village | T1 SQ95 Fushe Lura village | T2 GL32 Preja Lura | T2 SQ68 road to Gomsique, outcrop 3 | T2 SQ61 Mnela and Vigu areas, Kettalla | T3 GL28 Preja Lura | T3 SQ80 Fushe Lura village | T3 SQ82 Fushe Lura village | T4 SQ101 Fushe Lura village | T4 GL12 Gure Lura village | T4 GL14 Gure Lura village |
|--------------------------------|---|-----------------------------------|-------------------------------------|---|---|---|---|-------------------------------------|-------------------------------------|--|------------------------------------|---|
| Provenance | Gure Lura village | Gure Lura village | Fushe Lura village | Preja Lura | road to Gomsique, outcrop 3 | Mnela and Vigu areas, Kettalla | Preja Lura | Fushe Lura village | Fushe Lura village | Fushe Lura village | Gure Lura village | Gure Lura village |
| Lithology | Schistose Clzo- bearing amphibolite | Fine-grained amphibolite | Greenschist facies metabasite | Titanian Hbl- bearing amphibolite | Cpx- bearing coarse-grained amphibolite | Cpx- bearing amphibolite | Grt- bearing coarse-grained amphibolite | Cpx- Grt- bearing amphibolite | Cpx- Grt- bearing amphibolite | Fine to medium grained amphibolite | Hornblende-rich amphibolite | Aegirine augite - bearing amphibolite |
| Oxide (wt%) | | | | | | | | | | | | |
| SiO ₂ | 49.50 | 47.20 | 48.07 | 47.40 | 49.42 | 49.19 | 53.50 | 45.67 | 45.73 | 50.9 | 35.3 | 45.9 |
| TiO ₂ | 1.88 | 2.27 | 1.72 | 0.98 | 0.35 | 0.89 | 1.81 | 1.40 | 1.46 | 1.94 | 5.07 | 3.28 |
| Al ₂ O ₃ | 13.10 | 13.20 | 12.74 | 15.80 | 17.33 | 15.78 | 15.20 | 13.54 | 12.82 | 15.18 | 12.6 | 17.4 |
| Fe ₂ O ₃ | 13.90 | 15.30 | 14.01 | 9.28 | 4.78 | 9.01 | 11.20 | 11.24 | 11.95 | 10.36 | 18.8 | 10.6 |
| Cr ₂ O ₃ | 0.02 | 0.17 | n.a. | 0.05 | n.a. | n.a. | <0.01 | n.a. | n.a. | n.a. | 0.01 | 0.01 |
| MgO | 6.39 | 6.89 | 9.06 | 6.44 | 10.33 | 9.26 | 5.30 | 9.34 | 10.41 | 2.97 | 7.06 | 1.8 |
| MnO | 0.19 | 0.25 | 0.18 | 0.15 | 0.10 | 0.14 | 0.23 | 0.18 | 0.19 | 0.14 | 0.26 | 0.15 |
| CaO | 10.10 | 9.95 | 9.89 | 13.80 | 11.56 | 10.52 | 7.94 | 14.14 | 13.25 | 8.22 | 13.7 | 12.9 |
| Na ₂ O | 1.88 | 3.01 | 2.27 | 2.60 | 2.91 | 3.05 | 2.21 | 2.00 | 1.88 | 3.35 | 1.58 | 3.72 |
| K ₂ O | 0.31 | 0.35 | 0.29 | 0.45 | 0.34 | 0.30 | 1.33 | 0.68 | 0.30 | 4.21 | 1.44 | 1.24 |
| P ₂ O ₅ | 0.15 | 0.20 | 0.19 | 0.08 | 0.03 | 0.13 | 0.31 | 0.15 | 0.18 | 1.13 | 1.56 | 1.02 |
| LOI | 2.65 | 1.40 | 1.58 | 1.65 | 2.84 | 1.71 | 0.95 | 1.66 | 1.83 | 1.6 | 2.15 | 1.55 |
| Sum | 100.07 | 100.2 | 100.0 | 98.7 | 100.0 | 100.0 | 100.1 | 100.0 | 100.0 | 100.0 | 99.5 | 99.6 |
| Trace Element (ppm) | | | | | | | | | | | | |
| Ba | 124 | 133 | 112 | 85 | 49 | 40 | 174 | 172 | 102 | 977 | 350 | 364 |
| Co | 47 | 47 | n.a. | n.a. | n.a. | n.a. | n.a. | n.a. | n.a. | n.a. | 51 | 44 |
| Cr | n.a. | n.a. | 227 | n.a. | 756 | 344 | n.a. | 420 | 430 | 16 | n.a. | n.a. |
| Cs | 0.9 | 0.9 | n.a. | n.a. | n.a. | n.a. | n.a. | n.a. | n.a. | n.a. | 0.9 | 2 |
| Cu | 62.6 | 56 | n.a. | n.a. | n.a. | n.a. | n.a. | n.a. | n.a. | n.a. | 1.6 | <0.5 |
| Hf | 0.9 | 6 | n.a. | n.a. | n.a. | n.a. | n.a. | n.a. | n.a. | n.a. | 7 | 0.9 |
| Nb | 9 | 26 | 3 | 2 | 2 | 5 | 4 | 2 | 1 | 59 | 102 | 66 |
| Ni | 56 | 57 | 85 | 137 | 143 | 146 | 37 | 116 | 129 | 22 | 76 | 12 |
| Pb | 9 | 11 | 2 | n.a. | 1 | 3 | n.a. | 5 | 4 | 8 | 14 | 16 |
| Rb | 9 | 9 | 8 | 2 | 10 | 6 | 33 | 15 | 3 | 76 | 14 | 22 |
| Sc | 41.1 | 47.8 | 51 | n.a. | 34 | 40 | n.a. | 50 | 51 | 16 | 34 | 16.9 |
| Sr | 155 | 75 | 153 | 287 | 272 | 170 | 222 | 212 | 204 | 306 | 189 | 765 |
| Ta | 0.9 | 0.9 | n.a. | n.a. | n.a. | n.a. | n.a. | n.a. | n.a. | n.a. | 8 | 6 |
| Th | 0.2 | 0.3 | 1 | 0.1 | 1 | 3 | 1.1 | 1 | 2.5 | 9 | 8.6 | 9.3 |
| U | 0.1 | 0.1 | 3 | 0.1 | 1 | 2.5 | 0.4 | 1 | 3 | 1 | 2.3 | 2.4 |
| V | 428 | 464 | n.a. | n.a. | n.a. | n.a. | n.a. | n.a. | n.a. | n.a. | 277 | 206 |
| W | 170 | 110 | n.a. | n.a. | n.a. | n.a. | n.a. | n.a. | n.a. | n.a. | 71 | 450 |
| Y | 45 | 50 | 43 | 26 | 10 | 21 | 41 | 28 | 32 | 37 | 77 | 37 |
| Zn | 81 | 101 | 122 | n.a. | 29 | 33 | n.a. | 84 | 94 | 134 | 140 | 57.5 |
| Zr | 125 | 160 | 125 | 45 | 18 | 72 | 108 | 72 | 80 | 316 | 274 | 404 |

Table 3 - Rare earth element (REE) abundance of Eastern (present work) and Western (Carosi et al., 1996) amphibolites.

| Type Sample | T1 GL17 Gure Lura village | T1 GL4 Gure Lura village | T1 SQ95 Fushe Lura village | T2 GL32 Preja Lura | T2 SQ68 road to Gomsique, outcrop 3 | T2 SQ61 Mnela and Vigu areas, Keftalla | T3 GL28 Preja Lura | T3 SQ80 Fushe Lura village | T3 SQ82 Fushe Lura village | T4 SQ101 Fushe Lura village | T4 GL12 Gure Lura village | T4 GL14 Gure Lura village |
|----------------------------------|--|-----------------------------------|-------------------------------------|---|---|---|---|-------------------------------------|-------------------------------------|--|------------------------------------|---|
| Provenance | Gure Lura village | Gure Lura village | Fushe Lura village | Preja Lura | Gomsique, outcrop 3 | Mnela and Vigu areas, Keftalla | Preja Lura | Fushe Lura village | Fushe Lura village | Fushe Lura village | Gure Lura village | Gure Lura village |
| Lithology | Schistose Clz- bearing amphibolite | Fine-grained amphibolite | Greenschist facies metabasite | Titanian Hbl- bearing amphibolite | Cpx- bearing coarse-grained amphibolite | Cpx- bearing amphibolite | Grt- bearing coarse-grained amphibolite | Cpx- Grt- bearing amphibolite | Cpx- Grt- bearing amphibolite | Fine to medium grained amphibolite | Hornblende-rich amphibolite | Aegitine augite - bearing amphibolite |
| Rare Earth Elements (ppm) | | | | | | | | | | | | |
| La | 3.2 | 4.2 | 3.4 | 2 | 1.1 | 5.07 | 12.2 | 3.68 | 3.64 | 54 | 67.4 | 64.3 |
| Ce | 11.5 | 14.4 | 11.1 | 5.6 | 2.9 | 9.91 | 16.7 | 11.79 | 11.78 | 116 | 172 | 125 |
| Pr | 2 | 2.5 | n.a. | 0.9 | n.a. | n.a. | 3.9 | n.a. | n.a. | n.a. | 23.5 | 15.2 |
| Nd | 11.8 | 13.3 | 10.7 | 5.6 | 2.1 | 6.82 | 20.5 | 9.13 | 9.4 | 50 | 94.3 | 55.9 |
| Sm | 4.2 | 4.4 | 4.3 | 2.2 | 0.8 | 2.01 | 5.7 | 2.98 | 3.35 | 10.7 | 20 | 10.8 |
| Eu | 1.45 | 1.61 | 1.34 | 0.85 | 0.41 | 0.81 | 1.86 | 1.09 | 1.2 | 3.07 | 6.19 | 3.39 |
| Gd | 5.5 | 6.4 | 5.4 | 3 | 1 | 2.81 | 6.7 | 4.12 | 4.89 | 9.28 | 20.1 | 10.7 |
| Tb | 1 | 1.2 | n.a. | 0.5 | n.a. | n.a. | 1 | n.a. | n.a. | n.a. | 2.8 | 1.5 |
| Dy | 6.9 | 7.9 | n.a. | 3.9 | n.a. | 3.19 | 7.4 | 4.65 | 5.53 | 7.03 | 14 | 7.1 |
| Ho | 1.62 | 1.94 | n.a. | 0.73 | n.a. | n.a. | 1.43 | n.a. | n.a. | n.a. | 2.99 | 1.42 |
| Er | 4.6 | 5.2 | 4.5 | 2.5 | 0.9 | 1.83 | 4.5 | 2.76 | 3.56 | 3.54 | 7.2 | 3.6 |
| Tm | 0.6 | 0.7 | n.a. | 0.3 | n.a. | n.a. | 0.6 | n.a. | n.a. | n.a. | 0.9 | 0.4 |
| Yb | 4.4 | 5.4 | 4.3 | 2.3 | 0.8 | 1.8 | 4.2 | 2.64 | 3.32 | 2.94 | 5.5 | 2.9 |
| Lu | 0.63 | 0.75 | 0.61 | 0.32 | 0.07 | 0.3 | 0.61 | 0.38 | 0.54 | 0.4 | 0.77 | 0.38 |
| La _N /Sm _N | 0.47 | 0.59 | 0.49 | 0.56 | 0.85 | 1.56 | 1.32 | 0.76 | 0.67 | 3.11 | 2.08 | 3.67 |
| Gd _N /Yb _N | 1.00 | 0.94 | 1.00 | 1.04 | 1.00 | 1.24 | 1.27 | 1.24 | 1.17 | 2.52 | 2.91 | 2.94 |
| La _N /Yb _N | 0.49 | 0.52 | 0.53 | 0.58 | 0.92 | 1.88 | 1.94 | 0.93 | 0.73 | 12.28 | 8.19 | 14.83 |
| REE | 59.4 | 69.9 | 45.7 | 30.7 | 10.1 | 34.6 | 87.3 | 43.2 | 47.2 | 257.0 | 437.7 | 302.6 |
| Eu/Eu* | 0.93 | 0.93 | 0.85 | 1.02 | 1.41 | 1.05 | 0.93 | 0.96 | 0.91 | 0.95 | 0.95 | 0.97 |
| LREE | 28.5 | 34.4 | 0.85 | 14.1 | 6.1 | 21.8 | 53.3 | 24.6 | 24.8 | 220.0 | 357.2 | 260.4 |
| HREE | 10.2 | 12.1 | 9.4 | 5.4 | 1.8 | 3.9 | 9.9 | 5.8 | 7.4 | 6.9 | 14.4 | 7.3 |

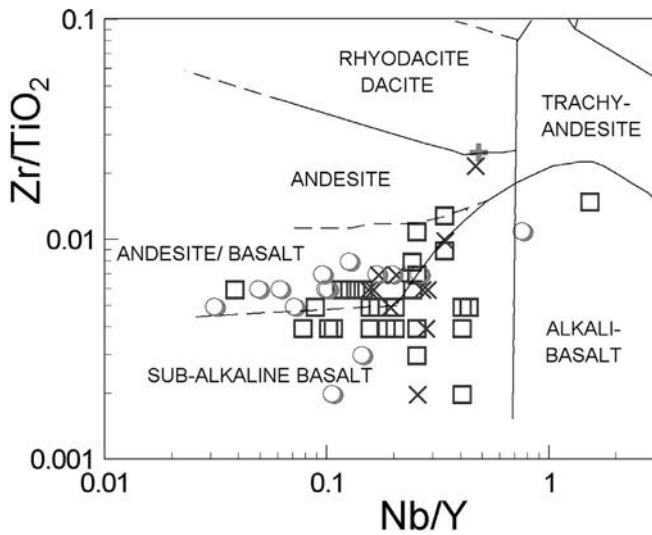


Fig. 4 - Zr/TiO₂ - Nb/Y (Winchester and Floyd, 1977) classification diagram. Symbols: diamond: T1; square: T2; circle: T3; triangle: T4; cross and oblique cross indicate rodingitic samples within T1 and T2, respectively.

(Σ LREE: 1.70-6.70 ppm) and positive Eu anomaly ($\text{Eu}/\text{Eu}^* = 0.19-0.53$) and II) a group with flat REE patterns and abundances about 10 chondrite (Σ REE: 22.83–34.55 ppm).

T3 amphibolites have a large compositional range; TiO₂,

P₂O₅, Zr and Y (Figure 5), are inversely correlated with Mg#, whereas a direct correlation is highlighted for Cr and Ni. In the classification diagram (Figure 4), the T3 amphibolites plot in the subalkaline basalt and andesite basalt fields. The REE patterns are relatively flat ($\text{LaN}/\text{YbN} = 0.15-1.94$); some of them show values less than 10 chondrite (Σ REE: 12.26-20.77 ppm) with low HREE (Σ HREE: 2.55-3.83 ppm), with negative or no LREE fractionation ($\text{LaN}/\text{SmN} = 0.19-0.66$). A second group of patterns has Σ REE in the range of 27.46-87.30 ppm, with Σ HREE: 4.02-9.91 ppm and no to positive LREE fractionation ($\text{LaN}/\text{SmN} = 4.02-9.91$). The T4 amphibolites are characterized by basaltic to trachy-basaltic compositions (TAS, not reported) in the alkalic basalt field (Figure 4). The modal hornblende plagioclase abundances largely account for the wide compositional range ($\text{Mg}\# = 14.52-57.27$, $\text{SiO}_2 = 33.7-50.9\text{wt}\%$, $\text{Al}_2\text{O}_3 = 8.9-17.4\text{wt}\%$ and $\text{K}_2\text{O} = 0.7-4.23\text{wt}\%$; Table 2d). Ba and Rb are high; TiO₂ (1.7-5.0wt%) and P₂O₅ (0.3-4.8wt%) are relatively high and inversely correlated with Mg# (Fig. 5), as well as Zr (131-404 ppm) and Y (23-77 ppm). Cr and Ni are relatively low and directly correlated with Mg#; Sr and, in part, Al₂O₃ and CaO increase as Mg# decreases whereas Sc decreases.

REE (Table 3d; Σ REE: 122.94-437.65 ppm) show parallel patterns, with marked fractionation ($\text{LaN}/\text{YbN} = 7.43-15.19$).

T4 amphibolites have a relatively wide compositional

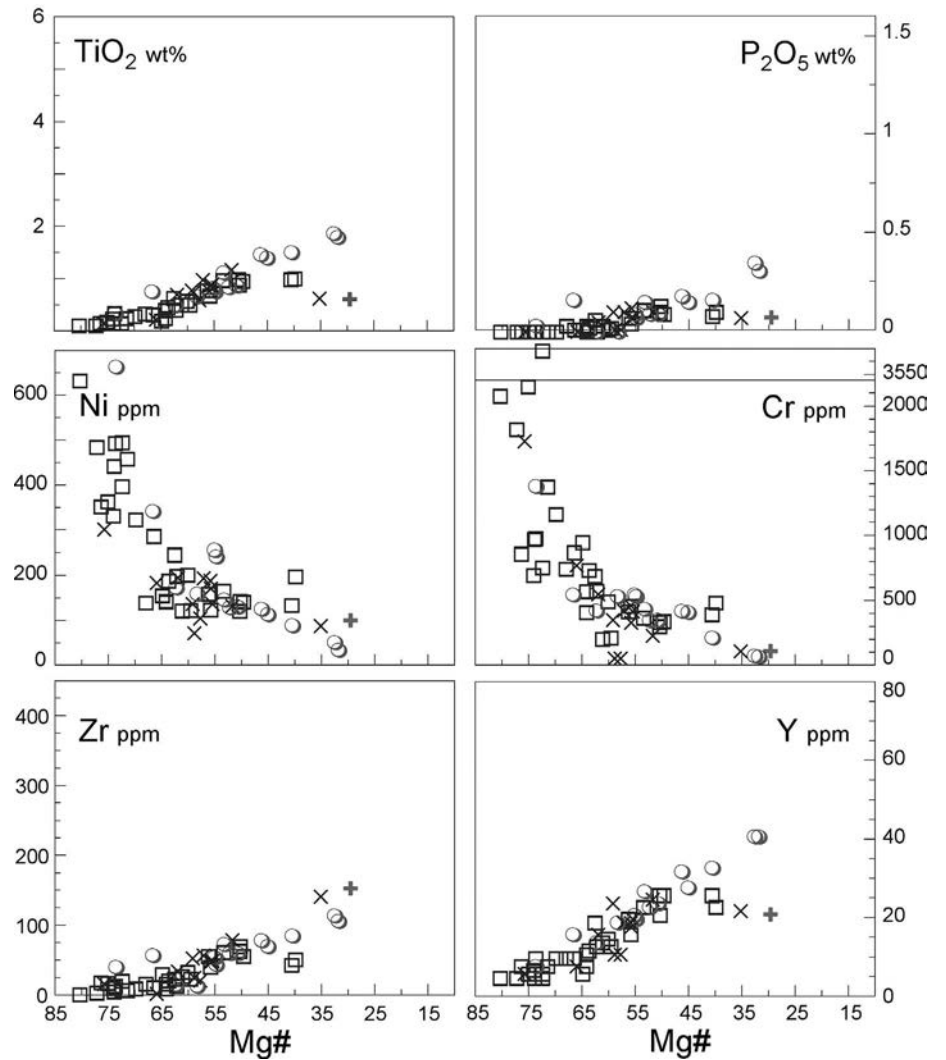


Fig. 5 - Selected oxide and element correlations vs. Mg#. Symbols as in Fig. 4.

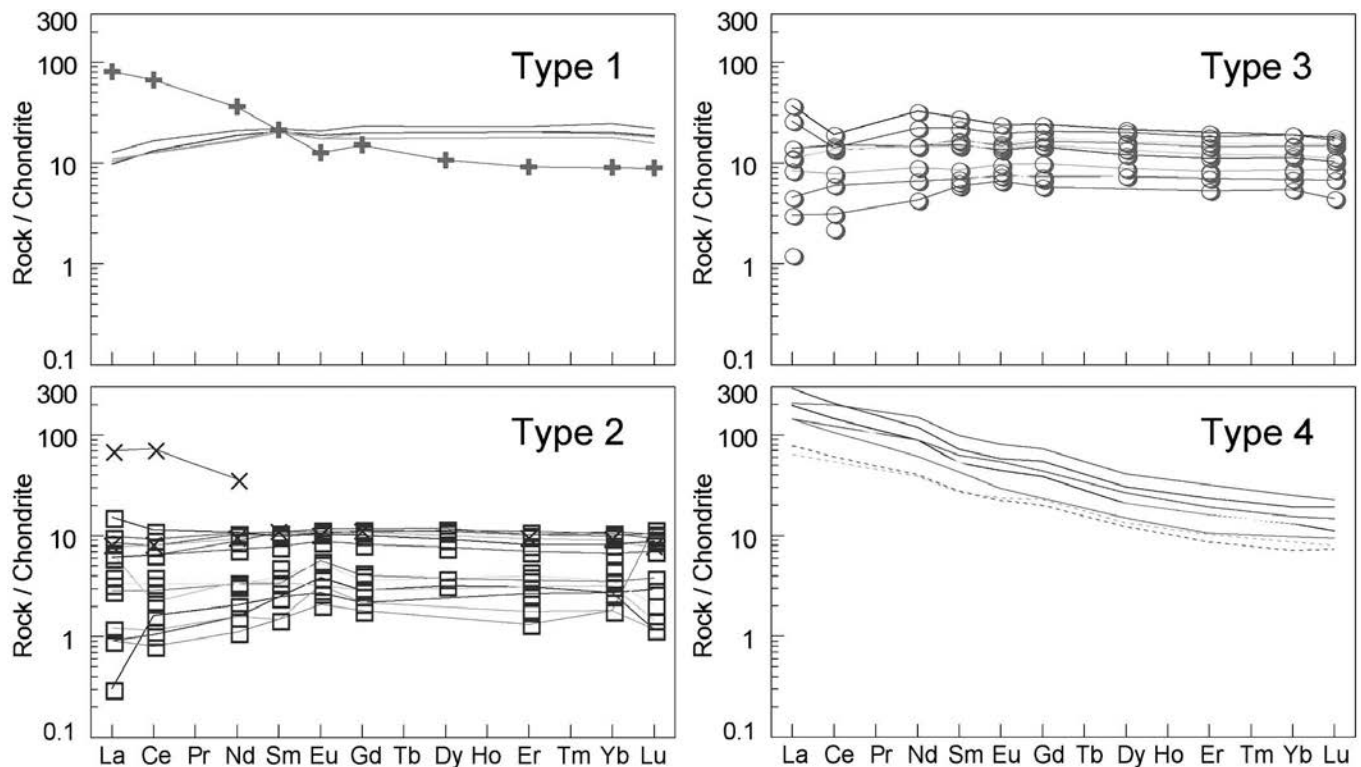


Fig. 6 - Chondrite-normalized REE patterns for T1-4 amphibolites (chondrite values after Nakamura, 1974).

range (Mg# between 14.52-57.27): samples with low trace and REE contents and high Mg and Ni. On the whole, the T4 amphibolites correspond to alkalic intraplate basalts. Gneisses and micaschists (Table 4) correspond to compositions between clays and graywackes (Carosi et al., 1996). NASC- (North American Shale Composite; Gromet et al., 1984) normalized multi-element diagrams (not reported) show relatively homogeneous compositions close to the average crust.

Genetic environment and secondary processes

The inference on the genetic environment for T1, T2 and T3 are based on field association and microtextural ground together with chemical features. As a fact T1 are fine-grained effusive metabasalts, whereas T2 and T3 are medium and in part coarse grained intrusive rocks. Despite the chemical signature of cumulus processes, the textural rehomogenization following to tectonics and the grain size allow comparing meta-effusive and -intrusive rocks

T1, T2 and T3 show an overall tholeiitic chemical affinity with LILE (mostly Rb and Ba) enrichment, which can be inferred as due to early seafloor alteration before the obduction. The significantly high U content (T1: 0.1- 4 ppm; T2: 0.1-5 ppm; T3: = 0.4-4 ppm) can also be due to incorporation in seawater or to local anomalies.

However, oxidation or enrichment trends typical of low-T seawater-rock interaction, expressed by 1) MgO enrichment in parallel with SiO₂ loss, due to palagonitization and/or 2) Ca loss and Na enrichment related to spilitization at subgreenschist facies temperatures, are not obvious. As a consequence, subseafloor alteration is considered to have induced only minor chemical mobilizations. Furthermore, a prevalent igneous heritage is suggested by the LILE and Nb correlation with the fractionation trends. On the whole, the gneisses point to a continental island-arc signature on the basis of the Th - Sc - Zr/10 diagram (Bhatia and Crook, 1986; Figure

7A), except for some samples characterized by lower Th/Sc and Sc/Zr. A detrital continental input is shown in the Roser and Korsch (1988) diagram (Figure 7B), where the gneisses fall into the quartzose sedimentary provenance field.

On the whole, the petrography and chemical features of the T1 amphibolites, and their tight association with metasediments, are consistent with an origin as extrusive protoliths. In contrast, the chemistry and relic textural features of T2 amphibolites are in accord with an origin from a cumulus gabbroic suite. The high abundances of MgO, Ni and Cr, associated with low P₂O₅, HFSE and REE in most samples and the poor REE fractionation with Eu positive anomaly are likewise referable to olivine + plagioclase + Cr-spinel cumulus. The increase of HFSE and Sc in samples at decreasing Mg# matches clinopyroxene precipitation. An origin in intrusive protoliths affected by olivine fractionation and by consequent clinopyroxene, apatite and ilmenite enrichment in the more evolved compositions is inferred for the T3 amphibolites.

All the data, and in particular that referring to LREE and LILE enrichment relative to MORB, can be interpreted as indicative of OIT affinity for the magmas that originated in T1, T2 and T3. The OIB affinity of T1, T2 and T3 amphibolites also matches their distinctive ratios (Blum et al., 1996; Table 5) such as the low Zr/Nb (2.69-7.68, < 10 in OIB), K/Ba (23.89-70.23) Ti/Y (314.33-619.48), and P/Ce (26.59-42.86), Zr/Y (3.55-10.91) and Nb/Y (1.04-2.21). In the La/10-Y/15-Nb/8 (Cabanis and Lecolle, 1989; not reported), T1 and T3 amphibolites plot mostly in the enriched-MORB field, and have Nb/La far exceeding those of BABB.

The K/Na defines a potassic alkaline character for T4. Incompatible element abundances normalized to the primordial mantle (Figure 8) show important Ta, Nb, Nd and P spikes and Hf, Sr and K troughs, which match the HIMU-dominated OIBs (Weaver, 1991), that also arise from characteristic ratios (Table 2).

Table 4 - Major and trace element compositions of gneisses and micaschists associated with Eastern (present work, GL series) and Western (Carosi et al., 1996, SQ series) amphibolites.

| Provenance | Keffalla | Bottom M.Boka slope | Bottom M.Boka slope | Along Gomsique river | Fushe Lura village |
|--------------------------------|----------------------------|----------------------------|----------------------------|----------------------------|----------------------------|----------------------------|----------------------------|----------------------------|----------------------------|----------------------------|
| Sample | SQ53 | SQ62 | SQ63 | SQ78 | SQ84 | SQ85 | SQ86* | SQ87 | SQ87* | SQ88 |
| Lithology | Grt-bearing Qtz-micaschist |
| Oxide (wt%) | | | | | | | | | | |
| SiO ₂ | 78.78 | 59.05 | 69.65 | 63.02 | 57.38 | 60.83 | 58.84 | 62.17 | 59.72 | 60.81 |
| TiO ₂ | 0.42 | 0.85 | 0.60 | 0.76 | 0.91 | 0.79 | 0.84 | 0.81 | 0.80 | 0.86 |
| Al ₂ O ₃ | 10.25 | 19.88 | 15.56 | 16.77 | 19.57 | 18.37 | 19.18 | 15.20 | 18.54 | 17.40 |
| Fe ₂ O ₃ | 3.77 | 6.58 | 4.27 | 6.53 | 6.80 | 6.65 | 6.52 | 6.75 | 6.02 | 6.65 |
| MnO | 0.06 | 0.34 | 0.07 | 0.57 | 0.21 | 0.25 | 0.23 | 0.24 | 0.17 | 0.23 |
| MgO | 1.23 | 3.20 | 2.06 | 4.06 | 4.62 | 3.69 | 4.19 | 5.23 | 4.51 | 4.43 |
| CaO | 0.81 | 1.13 | 0.72 | 0.97 | 1.74 | 1.80 | 2.03 | 2.47 | 1.88 | 1.80 |
| Na ₂ O | 2.45 | 2.04 | 1.51 | 1.13 | 1.51 | 1.52 | 1.87 | 2.50 | 1.63 | 2.44 |
| K ₂ O | 0.62 | 2.97 | 3.05 | 3.38 | 3.97 | 3.18 | 3.20 | 1.97 | 3.32 | 2.74 |
| P ₂ O ₅ | 0.09 | 0.18 | 0.12 | 0.10 | 0.24 | 0.19 | 0.18 | 0.21 | 0.20 | 0.22 |
| LOI | 1.51 | 3.78 | 2.38 | 2.72 | 3.06 | 2.73 | 2.91 | 2.46 | 3.21 | 2.42 |
| Sum | 99.99 | 100.00 | 99.99 | 100.01 | 100.01 | 100.00 | 99.99 | 100.01 | 100.00 | 100.00 |
| Trace Element (ppm) | | | | | | | | | | |
| Ba | 108 | 518 | 424 | 281 | 525 | 437 | 403 | 291 | 491 | 782 |
| Ce | 20 | 50 | 43 | 74 | 73 | 51 | 49 | 54 | 47 | 95 |
| Cr | 68 | 110 | 88 | 82 | 129 | 103 | 106 | 112 | 120 | 327 |
| La | 10 | 26 | 29 | 30 | 20 | 13 | 11 | 16 | 12 | 35 |
| Nb | 9 | 17 | 13 | 14 | 16 | 15 | 16 | 14 | 14 | <3 |
| Nd | 10 | 19 | 15 | 25 | 20 | 12 | 12 | 16 | 12 | 29 |
| Ni | 30 | 56 | 19 | 82 | 94 | 79 | 83 | 83 | 81 | 87 |
| Pb | 15 | 27 | 9 | 28 | 27 | 26 | 26 | 25 | 24 | 32 |
| Rb | 26 | 101 | 56 | 91 | 101 | 94 | 102 | 94 | 87 | 7 |
| Sc | 7 | 19 | 15 | 18 | 13 | 17 | 15 | 17 | 15 | 49 |
| Sr | 95 | 135 | 77 | 62 | 92 | 86 | 90 | 126 | 71 | 100 |
| Th | 5 | 12 | 9 | 10 | 12 | 10 | 10 | 10 | 13 | 13 |
| U | 3 | 3 | 4 | 3 | 3 | <2 | 4 | 4 | 4 | 25 |
| Y | 13 | 23 | 14 | 21 | 22 | 25 | 24 | 23 | 20 | 32 |
| Zn | 45 | 84 | 51 | 103 | 115 | 90 | 90 | 94 | 92 | 140 |
| Zr | 200 | 184 | 236 | 139 | 183 | 187 | 183 | 165 | 203 | 97 |

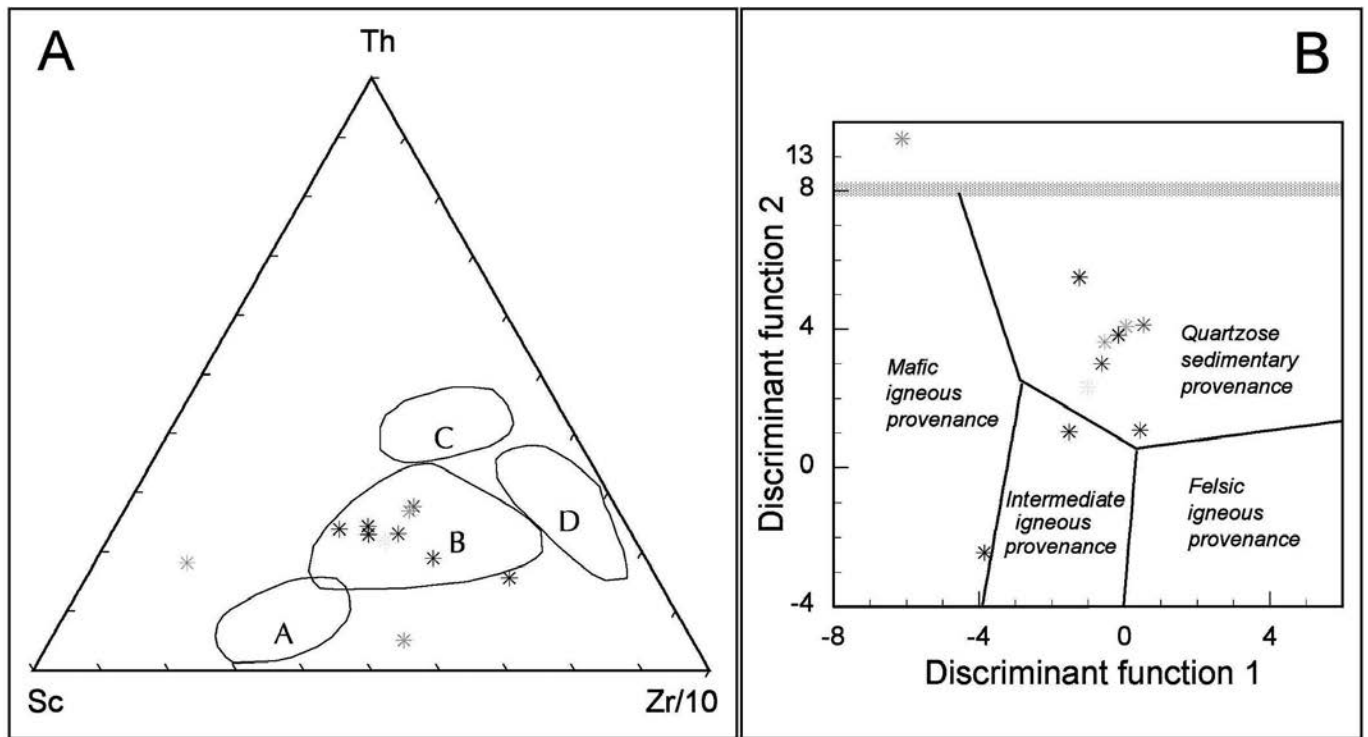


Fig. 7 - A: Th-Sc-Zr/10 diagram (Bhatia and Crook, 1986). Fields: A, oceanic island-arc; B, continental island-arc; C, active continental margin; D, passive margin. B: Discriminant function for the provenance signature (Roser and Korsch, 1988). Discriminant function 1 = $30.638\text{TiO}_2/\text{Al}_2\text{O}_3 - 12.541\text{Fe}_2\text{O}_3(\text{total})/\text{Al}_2\text{O}_3 + 7.329\text{MgO}/\text{Al}_2\text{O}_3 + 12.031\text{Na}_2\text{O}/\text{Al}_2\text{O}_3 + 35.402\text{K}_2\text{O}/\text{Al}_2\text{O}_3 - 6.382$, Discriminant function 2 = $56.500\text{TiO}_2/\text{Al}_2\text{O}_3 - 10.879\text{Fe}_2\text{O}_3(\text{total})/\text{Al}_2\text{O}_3 + 30.875\text{MgO}/\text{Al}_2\text{O}_3 - 5.404\text{Na}_2\text{O}/\text{Al}_2\text{O}_3 + 11.112\text{K}_2\text{O}/\text{Al}_2\text{O}_3 - 3.89$.

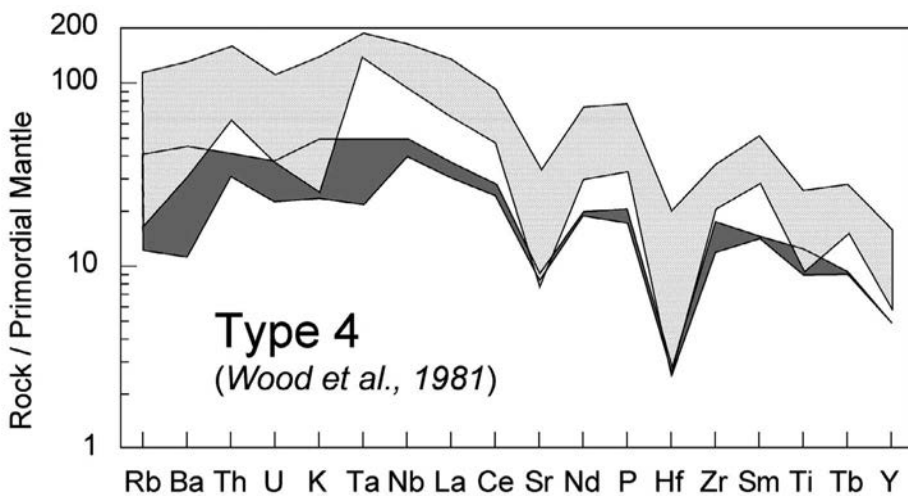


Fig. 8 - Incompatible element abundances normalized to primordial mantle (primordial mantle values after Wood et al., 1981) for T4 amphibolites. Gray pattern: samples GL15 and SQ83, hornblende cumulus composition. Hatched patterns: amphibole, plagioclase, K-feldspar, clinopyroxene ± biotite, + ilmenite + apatite compositions.

Table 5a - Significant trace and rare earth ratios of Eastern (present work) and Western (Carosi et al., 1996) amphibolites. Type 1.

| Sample | GL17 | GL4 | SQ18 | SQ18' | SQ50 | SQ92 | SQ93 | SQ95 | SQ96 |
|------------|------------------------------------|--------------------------|-----------------------|-----------------------|------------------------------------|-------------------------------|-------------------------------|-------------------------------|--------------------|
| Provenance | Gure Lura village | Gure Lura village | Rrethi j Eperm | Rrethi j Eperm | Along Gomsique river | Fushe Lura village | Fushe Lura village | Fushe Lura village | Fushe Lura village |
| Lithology | Schistose Clzo-bearing amphibolite | Fine-grained amphibolite | Mylonitic amphibolite | Mylonitic amphibolite | Rodingitized schistose amphibolite | Greenschist facies metabasite | Greenschist facies metabasite | Greenschist facies metabasite | Amphibolite |
| Zr/Nb | 13.9 | 6.2 | 64.0 | 38.0 | 15.4 | 54.0 | 63.5 | 41.7 | 51.5 |
| La/Nb | 0.36 | 0.16 | 0.50 | 0.33 | 2.65 | 1.80 | 0.50 | 1.13 | 1.50 |
| Ba/Nb | 13.8 | 5.1 | 85.0 | 12.3 | 3.0 | 12.0 | 8.0 | 37.3 | 12.0 |
| Ba/Th | 620.0 | 443.3 | 48.6 | 18.5 | 2.7 | 24.0 | 8.0 | 112.0 | 24.0 |
| Rb/Nb | 1.00 | 0.35 | 3.00 | 1.00 | 0.30 | 1.50 | 1.50 | 2.67 | 1.50 |
| K/Nb | 285.9 | 111.7 | 1618.7 | 387.4 | 8.3 | 954.6 | 954.6 | 802.4 | 498.1 |
| Th/Nb | 0.02 | 0.01 | 1.75 | 0.67 | 1.10 | 0.50 | 1.00 | 0.33 | 0.50 |
| Th/La | 0.06 | 0.07 | 3.50 | 2.00 | 0.42 | 0.28 | 2.00 | 0.29 | 0.33 |
| Ba/La | 38.8 | 31.7 | 170.0 | 37.0 | 1.1 | 6.7 | 16.0 | 32.9 | 8.0 |

Table 5b - Significant trace and rare earth ratios of Eastern (present work) and Western (Carosi et al., 1996) amphibolites. Type 2.

| Sample | GL8 | GL32 | GL22 | SQ4* | SQ4** | SQ4b | SQ9* | SQ40* | SQ47** | SQ48 | SQ49 | SQ52 | SQ57 |
|------------|------------------------------|----------------------------------|--------------------------------|-----------------------|-------------------------------------|-------------------------------|------------------------|----------------------------|-------------------------|----------------------------|----------------------------|----------------------------|-------------|
| Provenance | Gure Lura village | Preja Lura | Preja Lura | Road to Gomsique | Road to Gomsique | Road to Gomsique | Road to Gomsique | Along Gomsique river | Along Gomsique river | Along Gomsique river | Along Gomsique river | Keftalla | Keftalla |
| Lithology | Retrograde augen amphibolite | Titanian Hbl-bearing amphibolite | Cpx- Clizo-bearing amphibolite | Mylonitic amphibolite | Roddingitized mylonitic amphibolite | Weakly retrograde amphibolite | Retrograde amphibolite | Coarse-grained amphibolite | Cataclastic amphibolite | Coarse-grained amphibolite | Coarse-grained amphibolite | Coarse-grained amphibolite | Amphibolite |
| Zr/Nb | 3.6 | 22.5 | 26.5 | 17.5 | 13.8 | 9.5 | 10.0 | 3.5 | 14.5 | 9.0 | 6.5 | 11.0 | 19.3 |
| La/Nb | 0.01 | 1.00 | 1.40 | 0.50 | 0.50 | 0.50 | 0.15 | 0.20 | 0.50 | 0.65 | 0.50 | 0.94 | 1.08 |
| Ba/Nb | 11.8 | 42.5 | 45.0 | 19.0 | 6.0 | 16.5 | 135.5 | 6.5 | 16.0 | 34.0 | 97.5 | 82.0 | 11.3 |
| Ba/Th | 1177.8 | 850.0 | 180.0 | 38.0 | 24.0 | 33.0 | 271.0 | 6.5 | 16.0 | 17.0 | 195.0 | 82.0 | 11.3 |
| Rb/Nb | 1.56 | 1.00 | 5.50 | 1.50 | 0.75 | 1.50 | 5.50 | 1.50 | 1.50 | 6.50 | 11.00 | 8.00 | 1.67 |
| K/Nb | 433.5 | 1867.7 | 3444.9 | 871.6 | 83.0 | 498.1 | 1494.2 | 83.0 | 207.5 | 1743.2 | 2490.3 | 2739.3 | 1051.5 |
| Th/Nb | 0.01 | 0.05 | 0.25 | 0.50 | 0.25 | 0.50 | 0.50 | 1.00 | 1.25 | 1.00 | 1.00 | 1.00 | 1.00 |
| Th/La | 0.90 | 0.05 | 0.18 | 1.00 | 0.50 | 1.00 | 3.33 | 5.00 | 2.00 | 3.08 | 1.00 | 1.06 | 0.92 |
| Ba/La | 1060.0 | 42.5 | 32.1 | 38.0 | 12.0 | 33.0 | 903.3 | 32.5 | 32.0 | 52.3 | 195.0 | 87.2 | 10.5 |

| Sample | SQ60 | SQ64 | SQ65* | SQ68 | SQ45 | SQ4** | SQ4** | SQ35 | SQ35a | SQ36** | SQ44 | SQ47 | SQ4 |
|------------|-------------|---------------------|---------------------|--|----------------------------|-------------------------------------|-------------------------------------|--|--|---|----------------------------|---------------------------------------|-----------------------------|
| Provenance | Keftalla | Bottom M Boka slope | Bottom M Boka slope | Road to Gomsique | Along Gomsique river | Road to Gomsique | Road to Gomsique | Road to Gomsique, outcrop near lake of Shkoder | Road to Gomsique, outcrop near lake of Shkoder | Western side to Gomsique river, 5 km SW Kcire village | Along Gomsique river | Along Gomsique river | Road to Gomsique, outcrop 1 |
| Lithology | Amphibolite | Amphibolite | Amphibolite | Cpx-bearing coarse-grained amphibolite | Coarse-grained amphibolite | Roddingitized mylonitic amphibolite | Roddingitized mylonitic amphibolite | Roddingitized mylonitic amphibolite | Roddingitized mylonitic amphibolite | Roddingitized mylonitic amphibolite | Coarse-grained amphibolite | Roddingitized cataclastic amphibolite | Mylonitic amphibolite |
| Zr/Nb | 65.0 | 4.5 | 2.5 | 9.0 | 11.5 | 16.2 | 11.8 | 9.0 | 7.7 | 2.0 | 17.0 | 14.3 | 11.6 |
| La/Nb | 7.00 | 1.10 | 1.00 | 0.55 | 1.00 | 0.80 | 0.80 | 0.50 | 1.33 | 0.50 | 0.33 | 2.30 | 0.40 |
| Ba/Nb | 36.0 | 15.5 | 7.0 | 24.5 | 14.0 | 3.2 | 4.6 | 5.5 | 5.0 | 5.0 | 22.3 | 4.0 | 4.4 |
| Ba/Th | 12.0 | 15.5 | 7.0 | 49.0 | 11.2 | 16.0 | 23.0 | 11.0 | 7.5 | 4.0 | 33.5 | 3.6 | 8.8 |
| Rb/Nb | 7.00 | 1.50 | 1.50 | 5.00 | 1.50 | 5.00 | 0.60 | 1.50 | 1.00 | 1.50 | 1.00 | 0.60 | 0.50 |
| K/Nb | 2988.4 | 498.1 | 83.0 | 1411.2 | 539.6 | 116.2 | 99.6 | 41.5 | 27.7 | 124.5 | 110.7 | 0.0 | 99.6 |
| Th/Nb | 3.00 | 1.00 | 1.00 | 0.50 | 1.25 | 0.20 | 0.20 | 0.33 | 0.67 | 1.25 | 0.67 | 1.10 | 0.50 |
| Th/La | 0.43 | 0.91 | 1.00 | 0.91 | 1.25 | 0.25 | 0.25 | 0.38 | 0.50 | 2.50 | 2.00 | 0.48 | 1.25 |
| Ba/La | 5.1 | 14.1 | 7.0 | 44.5 | 14.0 | 4.0 | 5.8 | 11.0 | 3.8 | 10.0 | 67.0 | 1.7 | 11.0 |

| Sample | SQ20 | SQ20* | SQ25 | SQ25* | SQ65 | SQ2 | SQ38 | SQ38* | SQ42 | SQ61 | SQ66 | SQ67 | SQ86 | SQ102 |
|------------|------------------------|--------------------------------------|-----------------------|--------------------------------------|---------------------|--|----------------------|--|--|--|--|--|-----------------------|-------------------------|
| Provenance | Rraja e Velles | Rraja e Velles | Rraja e Velles | Rraja e Velles | Bottom M Boka slope | Road to Gomsique, outcrop near lake of Shkoder | Along Gomsique river | Along Gomsique river | Along Gomsique river | Mnela and Vigu areas, Keftalla | Mnela and Vigu areas, Keftalla | Road to Gomsique | Fushe Lura village | Fushe Lura village |
| Lithology | Retrograde amphibolite | Roddingitized retrograde amphibolite | Mylonitic amphibolite | Roddingitized retrograde amphibolite | Amphibolite | Roddingitized retrograde amphibolite | Amphibolite | Cpx-bearing coarse-grained amphibolite | Cpx-bearing coarse-grained amphibolite | Cpx-bearing coarse-grained amphibolite | Cpx-bearing coarse-grained amphibolite | Cpx-bearing coarse-grained amphibolite | Mylonitic amphibolite | Cpx-bearing amphibolite |
| Zr/Nb | 11.5 | 10.2 | 4.0 | 16.3 | 11.0 | 12.0 | 7.5 | 5.5 | 12.5 | 14.4 | 1.5 | 7.5 | 21.0 | 12.5 |
| La/Nb | 0.73 | 0.80 | 1.00 | 2.33 | 0.15 | 1.17 | 1.00 | 0.50 | 1.25 | 1.01 | 1.50 | 3.50 | 2.00 | 1.01 |
| Ba/Nb | 3.3 | 3.4 | 4.3 | 7.3 | 4.5 | 3.0 | 7.3 | 4.5 | 15.0 | 41.5 | 9.5 | 8.0 | 37.5 | 8.0 |
| Ba/Th | 5.1 | 17.0 | 5.2 | 22.0 | 3.0 | 9.0 | 19.0 | 41.5 | 15.0 | 13.3 | 6.3 | 46.0 | 37.5 | 16.0 |
| Rb/Nb | 0.55 | 0.60 | 1.00 | 1.00 | 1.50 | 1.00 | 1.50 | 6.50 | 1.50 | 1.20 | 0.50 | 10.00 | 2.50 | 1.50 |
| K/Nb | 150.9 | 149.4 | 138.4 | 166.0 | 83.0 | 55.3 | 124.5 | 1660.2 | 124.5 | 498.1 | 41.5 | 2780.8 | 1618.7 | 539.6 |
| Th/Nb | 0.64 | 0.20 | 0.83 | 0.33 | 1.50 | 0.33 | 0.50 | 1.00 | 1.00 | 0.60 | 1.50 | 1.00 | 1.00 | 0.50 |
| Th/La | 0.88 | 0.25 | 0.83 | 0.14 | 10.00 | 0.29 | 0.50 | 2.00 | 0.80 | 0.59 | 1.00 | 0.29 | 0.50 | 0.50 |
| Ba/La | 4.5 | 4.3 | 4.3 | 3.1 | 30.0 | 2.6 | 9.5 | 83.0 | 12.0 | 7.9 | 6.3 | 13.1 | 18.8 | 7.9 |

Table 5c - Significant trace and rare earth ratios of Eastern (present work) and Western (Carosi et al., 1996) amphibolites. Type 3.

| Sample | GL28 | GL35 | SQ8 | SQ55 | SQ56 | SQ56* | SQ26 | SQ35b | SQ35''' | SQ81 | SQ26' | SQ3 | SQ80 | SQ82 |
|------------|--|-------------------------|------------------------|-------------|-------------|-------------|-------------------------|--|--|-------------------------|-------------------------|-------------------------|------------------------------|------------------------------|
| Provenance | Preja Lura | Preja Lura | road to Gomsique | Keftalla | Keftalla | Keftalla | near Lake of Shkoder | road to Gomsique, outcrop near lake of Shkoder | road to Gomsique, outcrop near lake of Shkoder | Fushe Lura village | near Lake of Shkoder | road to Gomsique | Fushe Lura Village | Fushe Lura Village |
| Lithology | Grt-bearing coarse-grained amphibolite | Grt-bearing amphibolite | Retrograde amphibolite | Amphibolite | Amphibolite | Amphibolite | Amphibolite - granulite | Cpx-bearing amphibolite | Cpx-bearing amphibolite | Cpx-bearing amphibolite | Amphibolite - granulite | Cpx-bearing amphibolite | Cpx- Grt-bearing amphibolite | Cpx- Grt-bearing amphibolite |
| Zr/Nb | 27.0 | 58.0 | 29.5 | 10.7 | 28.0 | 23.0 | 8.5 | 13.8 | 15.5 | 43.5 | 7.5 | 7.0 | 36.0 | 80.0 |
| La/Nb | 3.05 | 4.30 | 0.75 | 0.66 | 1.38 | 4.50 | 0.20 | 0.22 | 0.25 | 1.86 | 0.50 | 0.83 | 1.84 | 3.64 |
| Ba/Nb | 43.5 | 42.0 | 4.5 | 4.3 | 24.0 | 26.0 | 21.0 | 12.7 | 13.8 | 115.0 | 21.0 | 3.0 | 86.0 | 102.0 |
| Ba/Th | 158.2 | 93.3 | 3.3 | 15.0 | 48.0 | 52.0 | 12.0 | 28.5 | 55.0 | 115.0 | 42.0 | 9.0 | 172.0 | 40.8 |
| Rb/Nb | 8.25 | 15.50 | 1.50 | 1.14 | 1.50 | 1.50 | 4.00 | 2.44 | 2.50 | 5.50 | 1.50 | 0.50 | 7.50 | 3.00 |
| K/Nb | 2760.1 | 4690.1 | 124.5 | 320.2 | 664.1 | 705.6 | 996.1 | 830.1 | 933.9 | 3112.9 | 41.5 | 96.8 | 2822.3 | 2490.3 |
| Th/Nb | 0.28 | 0.45 | 1.35 | 0.29 | 0.50 | 0.50 | 1.75 | 0.44 | 0.25 | 1.00 | 0.50 | 0.33 | 0.50 | 2.50 |
| Th/La | 0.09 | 0.10 | 1.80 | 0.43 | 0.36 | 0.11 | 8.75 | 2.00 | 1.00 | 0.54 | 1.00 | 0.40 | 0.27 | 0.69 |
| Ba/La | 14.3 | 9.8 | 6.0 | 6.5 | 17.5 | 5.8 | 105.0 | 57.0 | 55.0 | 62.0 | 42.0 | 3.6 | 46.7 | 28.0 |

Table 5d - Significant trace and rare earth ratios of Eastern (present work) and Western (Carosi et al., 1996) amphibolites. Type 4. For comparison, average N-MORB and range of HIMU OIB, EMII OIB, EMII OIB trace element ratios (Weaver, 1991).

| Sample | SQ101 | GL3 | GL12 | GL13 | GL14 | GL15 | GL14 | SQ103 | SQ83 | SQ83 | EMII OIB | EMII OIB | EMII OIB | EMII OIB |
|------------|------------------------------------|------------------------------|------------------------------|----------------------------|------------------------------------|--------------------------|----------------------------|------------------------------------|--------------------|--------------------|---------------|---------------|---------------|----------|
| Provenance | Fushe Lura village | Gure Lura village | Gure Lura village | Gure Lura village | Gure Lura village | Gure Lura village | Gure Lura village | Gure Lura village | Fushe Lura village | Fushe Lura village | Weaver, 1991 | | | |
| Lithology | Fine to medium-grained amphibolite | Retrograde augen amphibolite | Retrograde augen amphibolite | Horblende-rich amphibolite | Green Hbl-rich cumulus amphibolite | Cizo-bearing amphibolite | Medium-grained amphibolite | Coarse-grained cumulus amphibolite | | | N-MORB | HIMU OIB | EMII OIB | EMII OIB |
| Zr/Nb | 5.4 | 3.9 | 2.7 | 4.4 | 6.1 | 7.7 | 6.1 | 3.6 | 4.2 | 30 | 2.7 - 5.5 | 3.5 - 13.1 | 4.4 - 7.8 | |
| La/Nb | 0.92 | 0.49 | 0.66 | 1.15 | 0.97 | 0.84 | 0.97 | 0.76 | 0.83 | 1.07 | 0.64 - 0.82 | 0.78 - 1.32 | 0.79 - 1.19 | |
| Ba/Nb | 16.6 | 2.4 | 3.4 | 4.3 | 5.5 | 13.6 | 5.5 | 10.6 | 2.7 | 4.3 | 4.7 - 6.9 | 9.1 - 23.4 | 6.4 - 13.3 | |
| Ba/Th | 108.6 | 35.2 | 40.7 | 23.1 | 39.1 | 113.3 | 39.1 | 109.7 | 21.0 | 60 | 39 - 85 | 80 - 204 | 57 - 105 | |
| Rb/Nb | 1.29 | 0.11 | 0.14 | 0.18 | 0.33 | 1.08 | 0.33 | 0.98 | 0.26 | 0.36 | 0.30 - 0.43 | 0.69 - 1.41 | 0.58 - 0.87 | |
| K/Nb | 592.3 | 66.6 | 117.2 | 117.0 | 156.0 | 481.5 | 156.0 | 249.0 | 187.4 | 296 | 66 - 187 | 194 - 523 | 203 - 378 | |
| Th/Nb | 0.15 | 0.07 | 0.08 | 0.19 | 0.14 | 0.12 | 0.14 | 0.10 | 0.13 | 0.071 | 0.071 - 0.123 | 0.094 - 0.13 | 0.105 - 0.168 | |
| Th/La | 0.17 | 0.14 | 0.13 | 0.16 | 0.14 | 0.14 | 0.14 | 0.13 | 0.16 | 0.067 | 0.106 - 0.99 | 0.089 - 0.147 | 0.108 - 0.183 | |
| Ba/La | 18.1 | 4.8 | 5.2 | 3.8 | 5.7 | 16.1 | 5.7 | 14.0 | 3.3 | 4 | 6.2 - 9.3 | 11.3 - 19.1 | 7.3 - 13.5 | |

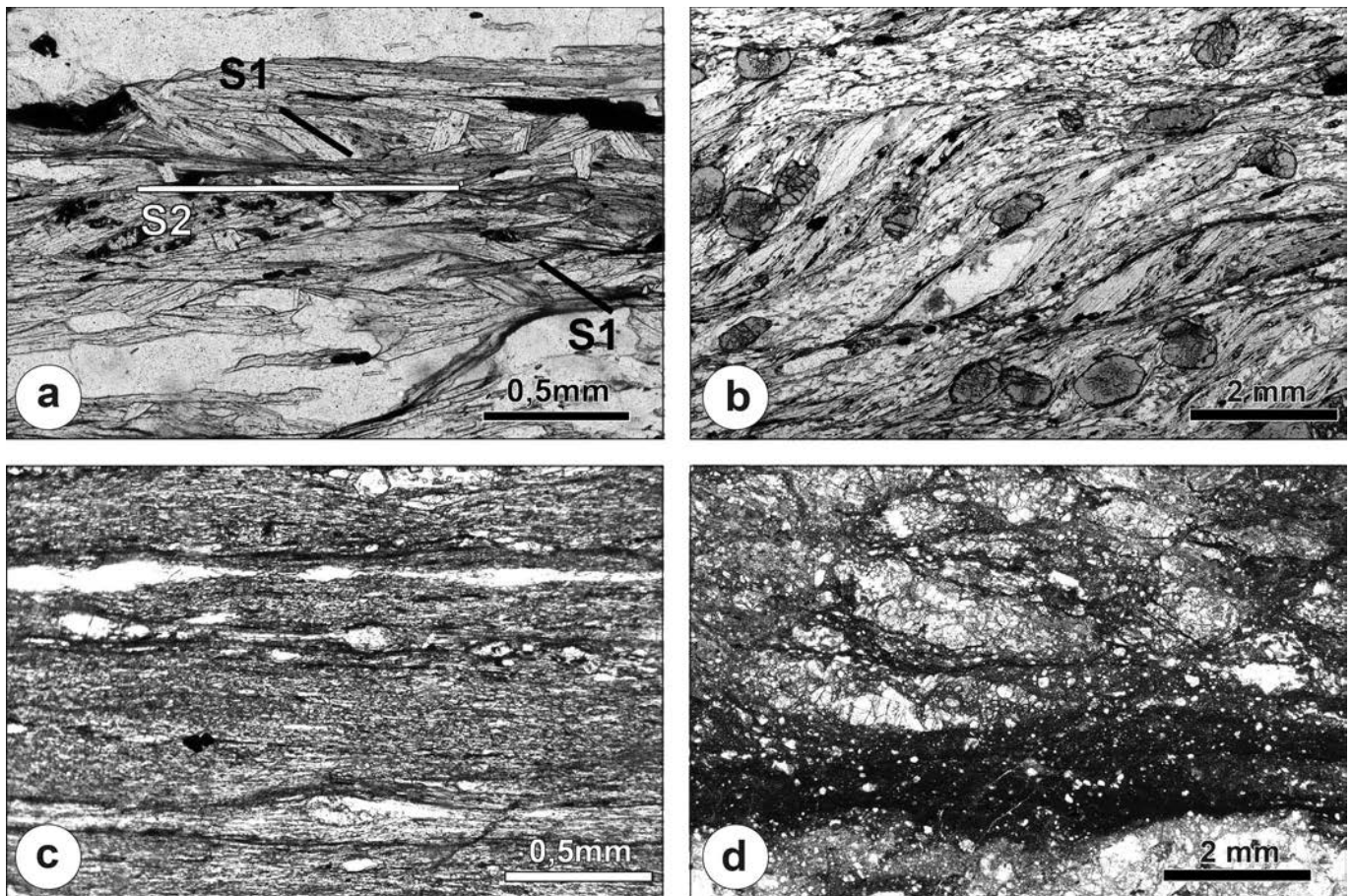


Fig. 9 - Photomicrographs of structures recognized in the metamorphic sole of the Mirdita ophiolitic Nappe. a) amphibolites characterized by S_2 schistosity defined by oriented plagioclase and amphiboles. Microlithons with relics of S_1 foliation are also shown; b) S-C structures in the garnet-bearing micaschists; c) mylonitic shear zone in amphibolite; d) cataclastic shear zone in amphibolite.

STRUCTURAL EVOLUTION: INSIGHTS ON THE ORIGIN OF THE METAMORPHIC SOLE

Structural evidences

The entire metamorphic sole experienced a complex structural history, well preserved at the meso- and microscopic scale. The intensity and degree of deformation vary in the different lithologies, although the structural evolution is similar to all of them and in both WOB and EOB. Generally, foliations and folds are pervasively developed in fine-grained rocks such as micaschists and fine-grained amphibolites, and less recorded in lithologies as the coarse-grained amphibolites.

All the amphibolite types can be described as L-S tectonites characterized by a well-developed, planar S_2 schistosity, associated with the D_2 phase. Centimetre-thick, banded mylonites occur in all amphibolites types parallel to the S_2 schistosity. In the WOB, the S_2 schistosity, generally steeply inclined toward the east, strikes from NW/SE to WNW/ESE. In the EOB, the S_2 schistosity shows a sharp N-S trend from Gure Lure to Preja Lure. The dip ranges from 30° to 60° toward the west. North of Preja Lure, the schistosity shows a NE/SW trend, probably resulting from rotation of about 30° by a strike slip fault. The S_2 schistosity in the metamorphic sole bears well developed L_2 mineral lineations. In the amphibolites, hornblende and plagioclase and, when present, clinopyroxene, are oriented or rotated on S_2 planes, whereas in the paragneisses and micaschists the mineral lineations are mainly represented by aligned mus-

covite and biotite. In the WOB the mineral lineation defines a clear ESE-WNW trend, whereas in the EOB the lineation strikes ENE-WSW. F_2 folds are rarely recognized in the coarse-grained T2 amphibolites, whereas they are more common in the micaschists and in the fine to medium-grained T1, T3 and T4 amphibolites. The F_2 folds have similar isoclinal folds, generally intrafolial and rootless, with rounded hinges and axial planes parallel to the S_2 schistosity. The F_2 folds can be defined as sheath folds showing fold hinge lines, reoriented on their axial planes parallel with the L_2 mineral lineations. Their amplitude ranges from several mm to a few cm, and no asymmetry can be observed.

A later D_3 phase can be recognized in T1 amphibolites, paragneisses and micaschists, but is poorly developed in the T2 amphibolites. The D_3 phase is characterized by chevron, tight to open folds with NW/SE axes. Their axial plane, generally showing eastward dip, is either a steep surface, as in the Gomsique area, or a weakly inclined plane, as in the Preja Lure area. The amplitude of the F_3 folds ranges from a few dm to several m, and a clear westward asymmetry can be observed in both the WOB and EOB. NW-SE axes and NW plunging characterize the F_3 folds. The F_3 folds are only associated with a poorly evolved S_3 axial plane crenulation cleavage in T1 amphibolites, paragneisses and micaschists. In these rocks the superimposed S_2/S_3 foliations produce a NW-SE intersection lineations very evident at the mesoscale. Traces of non-schistogenous folding are recognizable in the coarse-grained amphibolites, particularly where S_2 is most pervasive.

Non-foliated cataclasites with strong grain-size reduction and rounded porphyroclasts of amphibole and clinopyroxene developed in millimetre to centimetre-thick shear zones cutting the S_2 and S_3 foliations at a high angle. The cataclasites, together with a diffuse brittle deformation, associated with sub-greenschist metamorphic assemblages represent the last deformation structures affecting the metamorphic sole, and also the Rubik Complex.

In thin sections, the most striking feature of the metamorphic sole is a well-developed and widespread S_2 schistosity (Figure 9a). S_2 is generally defined by thin layers of oriented plagioclases alternating with bands enriched in syn-kinematic amphibole \pm clinopyroxene. The paragneisses and micaschists are also characterized by a main S_2 schistosity defined by thin bands of granoblastic plagioclase and quartz alternating with layers of lepidoblastic micas (Figure 9b).

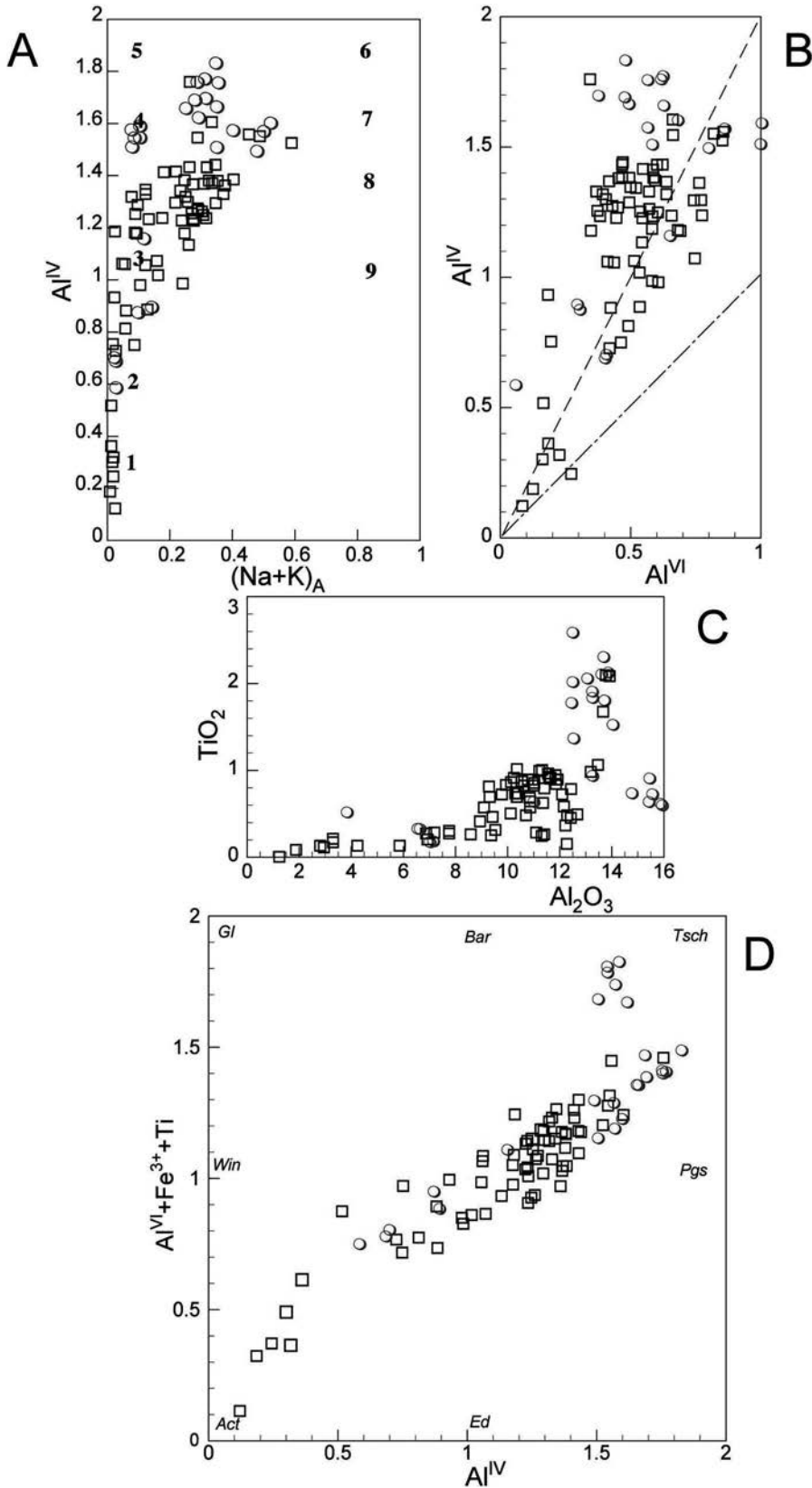


Fig. 10 - Significant cation and oxide correlations for T1-T4 amphiboles. A: Al^{IV} - (Na+K)_A (Bellot et al., 2003) 1: actinolite, 2: actinolitic hornblende, 3: hornblende, 4: tschermakitic hornblende, 5: tschermakite, 6: pargasite, 7: pargasitic hornblende, 8: edenitic hornblende, 9: edenite; B: Al^{IV} - Al^{VI} correlation; dashes: pargasite substitution. Dash-dot line: tschermakite substitution. C: TiO₂ - Al₂O₃; D: Al^{VI} + Fe³⁺ + Ti - Al^{IV}. Symbols: diamond: T1; square: T2; circle: T3; triangle: T4.

Table 6 - Mineral chemistry of selected amphiboles from Eastern (present work, GL series) and Western (Carosi et al., 1996, SQ series) amphibolites.

| Type | T1 | T1 | T1 | T2 | T2 | T2 | T2 | T2 | T2 | T3 | T3 | T3 | T3 | T3 | T4 | T4 | T4 | T4 | | |
|--------------------------------|-----------------------|---------------------------|-------------------------|-----------|---------------|---------------|---------------|---------------|-------------|-------------|--------------|-----------|-------------|--------------|-----------|-------------|--------------|-----------|-------------|--|
| Sample | SQ50 | SQ50 | SQ100 | GL32 | SO4' | SO42 | SO42 | SO56 | GL28 | GL29 | GL14 | GL12 | GL13 | GL14 | GL12 | GL13 | GL14 | GL13 | | |
| N. Analysis | PIA1 | PIA3 | PIA5 | PIA2 | P3A5 | P2A2 | P2A2 | PIA1 | PIA6 | PIA2 | P3A2 | PIA4 | PIA7 | P3A2 | PIA4 | PIA7 | P3A2 | PIA4 | PIA7 | |
| Classification | Mg-hornblende | Mg-hornblende | Mg-hornblende | Pargasite | Mg-hornblende | Mg-hornblende | Mg-hornblende | Mg-hornblende | Tschemakite | Tschemakite | Fe-pargasite | Pargasite | Tschemakite | Fe-pargasite | Pargasite | Tschemakite | Fe-pargasite | Pargasite | Tschemakite | |
| Occurrence | Coarse, pre-kinematic | Syn-kinematic small grain | Core of zoned amphibole | | | | | Coarse grain | | | | | | | | | | | | |
| Oxide (wt%) | | | | | | | | | | | | | | | | | | | | |
| SiO ₂ | 45.54 | 46.10 | 52.20 | 42.65 | 49.89 | 46.88 | 46.88 | 51.90 | 44.44 | 42.91 | 39.26 | 39.25 | 42.34 | 39.26 | 39.25 | 42.34 | 39.26 | 39.25 | 42.34 | |
| TiO ₂ | 0.43 | 0.63 | 0.23 | 2.09 | 0.27 | 1.00 | 1.00 | 0.32 | 0.59 | 1.90 | 2.16 | 1.43 | 1.97 | 2.16 | 1.43 | 1.97 | 2.16 | 1.43 | 1.97 | |
| Cr ₂ O ₃ | 0.23 | 0.19 | 0.30 | 0.16 | 0.13 | 0.16 | 0.16 | 0.48 | 0.13 | 0.23 | 0.19 | 0.18 | 0.16 | 0.19 | 0.18 | 0.16 | 0.19 | 0.18 | 0.16 | |
| Al ₂ O ₃ | 13.38 | 13.34 | 4.03 | 13.77 | 7.76 | 11.32 | 11.32 | 6.56 | 15.95 | 13.27 | 14.24 | 14.52 | 13.24 | 14.24 | 14.52 | 13.24 | 14.24 | 14.52 | 13.24 | |
| FeO | 14.27 | 13.36 | 12.78 | 14.10 | 11.72 | 11.09 | 11.09 | 9.34 | 14.13 | 13.24 | 20.92 | 18.08 | 15.48 | 20.92 | 18.08 | 15.48 | 20.92 | 18.08 | 15.48 | |
| MnO | 0.41 | 0.29 | 0.31 | 0.29 | 0.24 | 0.21 | 0.21 | 0.23 | 0.13 | 0.24 | 0.48 | 0.38 | 0.28 | 0.48 | 0.38 | 0.28 | 0.48 | 0.38 | 0.28 | |
| MgO | 11.12 | 11.47 | 15.24 | 10.81 | 14.60 | 13.94 | 13.94 | 16.10 | 9.55 | 11.05 | 6.03 | 8.65 | 10.19 | 6.03 | 8.65 | 10.19 | 6.03 | 8.65 | 10.19 | |
| NiO | 0.00 | 0.00 | 0.00 | 0.05 | 0.00 | 0.00 | 0.00 | 0.00 | 1.07 | 0.84 | 0.00 | 0.00 | 0.00 | 0.00 | 0.00 | 0.00 | 0.00 | 0.00 | 0.00 | |
| CaO | 11.02 | 11.06 | 11.68 | 12.36 | 12.34 | 12.13 | 12.13 | 12.39 | 11.83 | 12.02 | 11.46 | 11.50 | 11.26 | 11.46 | 11.50 | 11.26 | 11.46 | 11.50 | 11.26 | |
| Na ₂ O | 1.06 | 1.00 | 0.46 | 1.85 | 0.54 | 0.89 | 0.89 | 0.20 | 0.47 | 1.69 | 0.91 | 1.22 | 1.49 | 0.91 | 1.22 | 1.49 | 0.91 | 1.22 | 1.49 | |
| K ₂ O | 0.28 | 0.28 | 0.23 | 0.63 | 0.13 | 0.15 | 0.15 | 0.15 | 0.42 | 0.49 | 1.99 | 1.98 | 1.13 | 1.99 | 1.98 | 1.13 | 1.99 | 1.98 | 1.13 | |
| Total | 97.74 | 97.72 | 97.45 | 98.76 | 97.62 | 97.77 | 97.77 | 97.67 | 98.71 | 97.88 | 97.63 | 97.19 | 97.54 | 97.63 | 97.19 | 97.54 | 97.63 | 97.19 | 97.54 | |
| Cations | | | | | | | | | | | | | | | | | | | | |
| Si | 6.529 | 6.589 | 7.456 | 6.246 | 7.119 | 6.672 | 6.672 | 7.314 | 6.362 | 6.297 | 6.025 | 5.939 | 6.259 | 6.025 | 5.939 | 6.259 | 6.025 | 5.939 | 6.259 | |
| Ti | 0.046 | 0.068 | 0.025 | 0.230 | 0.029 | 0.107 | 0.107 | 0.034 | 0.064 | 0.210 | 0.250 | 0.163 | 0.219 | 0.250 | 0.163 | 0.219 | 0.250 | 0.163 | 0.219 | |
| Al ^{IV} | 1.471 | 1.411 | 0.544 | 1.524 | 0.881 | 1.328 | 1.328 | 0.687 | 1.575 | 1.493 | 1.725 | 1.898 | 1.522 | 1.725 | 1.898 | 1.522 | 1.725 | 1.898 | 1.522 | |
| Al ^{VI} | 0.790 | 0.836 | 0.133 | 0.853 | 0.424 | 0.571 | 0.571 | 0.403 | 1.117 | 0.802 | 0.852 | 0.691 | 0.785 | 0.852 | 0.691 | 0.785 | 0.852 | 0.691 | 0.785 | |
| Cr | 0.026 | 0.022 | 0.034 | 0.019 | 0.015 | 0.018 | 0.018 | 0.054 | 0.015 | 0.027 | 0.023 | 0.022 | 0.019 | 0.023 | 0.022 | 0.019 | 0.023 | 0.022 | 0.019 | |
| Fe ³⁺ | 0.830 | 0.702 | 0.583 | 0.118 | 0.439 | 0.552 | 0.552 | 0.339 | 0.556 | 0.282 | 0.421 | 0.647 | 0.510 | 0.421 | 0.647 | 0.510 | 0.421 | 0.647 | 0.510 | |
| Fe ²⁺ | 0.881 | 0.894 | 0.943 | 1.609 | 0.960 | 0.769 | 0.769 | 0.761 | 1.136 | 1.343 | 2.264 | 1.641 | 1.404 | 2.264 | 1.641 | 1.404 | 2.264 | 1.641 | 1.404 | |
| Mn | 0.050 | 0.035 | 0.037 | 0.036 | 0.029 | 0.025 | 0.025 | 0.028 | 0.016 | 0.030 | 0.062 | 0.049 | 0.035 | 0.062 | 0.049 | 0.035 | 0.062 | 0.049 | 0.035 | |
| Mg | 2.376 | 2.444 | 3.244 | 2.360 | 3.105 | 2.957 | 2.957 | 3.382 | 2.038 | 2.417 | 1.379 | 1.951 | 2.247 | 1.379 | 1.951 | 2.247 | 1.379 | 1.951 | 2.247 | |
| Ni | 0.000 | 0.000 | 0.000 | 0.006 | 0.000 | 0.000 | 0.000 | 0.000 | 0.123 | 0.099 | 0.000 | 0.000 | 0.000 | 0.000 | 0.000 | 0.000 | 0.000 | 0.000 | 0.000 | |
| Ca | 1.693 | 1.694 | 1.787 | 1.945 | 1.887 | 1.850 | 1.850 | 1.871 | 1.839 | 1.903 | 1.884 | 1.894 | 1.783 | 1.884 | 1.894 | 1.783 | 1.884 | 1.894 | 1.783 | |
| Na _R | 0.295 | 0.277 | 0.128 | 0.055 | 0.113 | 0.150 | 0.150 | 0.055 | 0.132 | 0.097 | 0.116 | 0.106 | 0.217 | 0.116 | 0.106 | 0.217 | 0.116 | 0.106 | 0.217 | |
| Na _A | 0.000 | 0.000 | 0.000 | 0.472 | 0.036 | 0.095 | 0.095 | 0.000 | 0.000 | 0.387 | 0.155 | 0.257 | 0.212 | 0.155 | 0.257 | 0.212 | 0.155 | 0.257 | 0.212 | |
| K | 0.051 | 0.051 | 0.042 | 0.118 | 0.024 | 0.027 | 0.027 | 0.027 | 0.078 | 0.092 | 0.390 | 0.388 | 0.213 | 0.390 | 0.388 | 0.213 | 0.390 | 0.388 | 0.213 | |

The shear sense of the metamorphic sole has been determined from the kinematic indicators, mainly C-type shear bands, mica fish and σ -type garnet porphyroblasts, evidenced in oriented thin sections. Generally, kinematic indicators are less clear in amphibolites, whereas in paragneisses and micaschists the shear sense can be easily determined. The metasedimentary rocks are generally characterized by a cleavage represented by shear bands that transect the mica-preferred orientation and the compositional layering at a low angle. The shear bands, generally of C-type, are mainly developed in the micaschists, where the mica fish structures, represented by lozenge-type, single grains of muscovite, are also widespread. Syn-tectonic σ -type garnet porphyroblasts with asymmetric pressure shadows are also common in the paragneisses. In the amphibolites the shear sense indicators are represented by syn-tectonic σ -type porphyroblasts of garnet and amphibole with asymmetric pressure shadows of fine-grained feldspar and amphibole fibers. The majority of these structures point to a clear top-to-W sense of shear in both the WOB and EOB (Figure 9c).

Relics of older structures are preserved at most places, mainly in the T2 and T3 amphibolites; relics of S_1 schistosity have also been identified in the T1 and T4 ones. At the micro-scale, the S_1 schistosity is generally preserved in lens-shaped centimeter to tens of meters-thick domains distinguishable by a broad, coarse-grained compositional banding. In addition, the S_2 schistosity transposes intrafolial, isoclinal folds that have been interpreted as remnants of the D_1 deformation phase. In the paragneisses and micaschists the textural remnants of an older schistosity are preserved in lens-shaped boudins of weakly oriented granoblastic quartz, plagioclase and mica aggregates. This may suggest a strain partitioning of the D_2 deformation resulted in a large scale struc-

ture where lenses characterized by prevailing coaxial deformation are surrounded by thin layers showing non-coaxial strain. Deformation partitioning was probably occurring during the whole deformation history of the amphibolites.

The D_1 and D_2 phases were followed by a D_3 phase characterized by greenschist facies overprint (Figure 9d).

THERMOBARIC CONSTRAINTS TO THE METAMORPHIC HISTORY

Mineral chemistry

Major elements in the mineral phases were analyzed at Genoa University using a Philips SEM 515 scanning electron microscope equipped with an EDAX PV9100 spectrometer in the energy-dispersive mode. Operating conditions were 15 kV accelerating voltage and 2.1 nA of beam current. The atomic proportions of pyroxene were calculated assuming stoichiometry and charge balance. The nomenclature follows the scheme of Morimoto et al. (1988), amplified by Rock (1990) for Na-Ca and Na-pyroxenes. Plagioclase was normalized to 5 cations and 8 oxygens. Garnet was recast to 5 cations and 12 oxygens. The epidote was normalized to 12.5 oxygens.

The nomenclature of Leake et al., (1997; 2003) revised by Hawthorne and Oberti (2007) was adopted (diagrams not reported). The Ca-amphibole cation sum was normalized to 13-(Ca+Na+K), as suggested by Laird and Albee (1981); $Fe^{3+} = 46$ -total cation charge and $Fe^{2+} = Fetot - Fe^{3+}$; $Al^{IV} = 8 - Si$, $Al^{VI} = Al_{tot} - Al^{IV}$. The mineral abbreviations follow Kretz (1983).

Amphibole

In T1, the amphiboles equilibrated at metamorphic peak are Mg-hornblendes to tschermakites (Table 6a) with low Mg# (0.55-0.63). The wide Al and (Na+K)A variation in a tschermakite substitution trend is highlighted in Figures 10A and B, the Ti content is relatively low (Figure 10C).

In T2, the amphiboles are Mg-hornblendes (Table 6b), with rare tschermakites and pargasites, all showing high Mg# (0.62-0.81). The Na content is relatively high and increases with Al^{IV} (Figure 10A). The TiO_2 content reaches 1 wt%.

In T3, the amphiboles are tschermakites, more rarely pargasites (Table 6c), characterized by either (I) prevalent tschermakite substitution, associated with a TiO_2 content of about 1 wt%, or (II) prevalent pargasite substitution, associated with TiO_2 in excess of 2 wt% (Figures 10A and D).

In T4, amphiboles are mostly tschermakites or pargasites, up to Fe-pargasites (Table 6d). The prevailing pargasite substitution associated with TiO_2 in the range 1 - 2.5 wt%, as shown in Figure 10A.

On the whole, the amphibole composition is in part controlled by the bulk rock, but the Al_2O_3 and TiO_2 contents likewise depend on the metamorphic parameters. The Al^{IV}/Al^{VI} are distributed, for the major part, along the pargasite vector (Figure 10B) and suggest intermediate temperature gradients (Fleet and Barnett, 1978).

Clinopyroxene

In T2, the clinopyroxenes are almost pure diopside, with low hedenbergite and appreciable enstatite ($En = 0.38-0.50$). In T3, they are diopside with appreciable hedenbergite and $En/Fs = 1.63-2.8$. In T4, the clinopyroxenes have higher Fe^{2+} and aegirine content in the range 7-11 mole% (Table 7a).

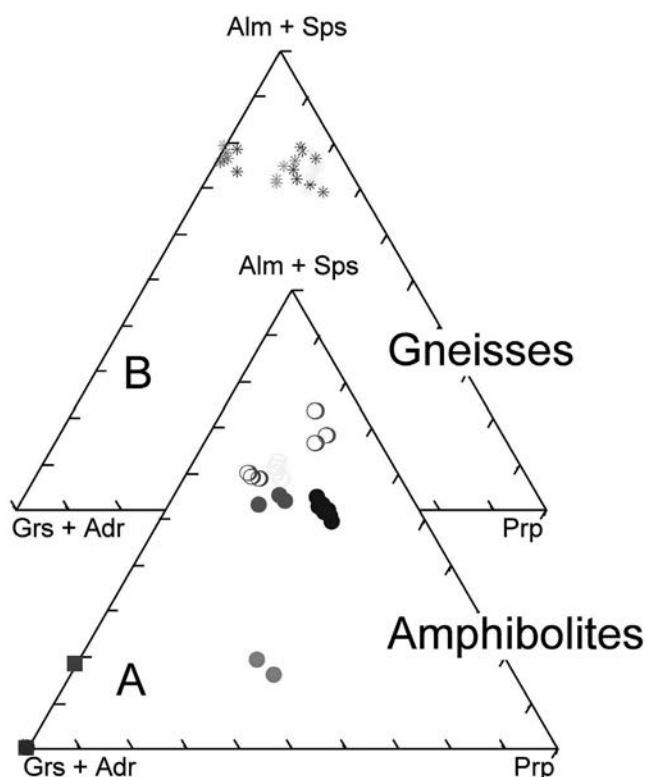


Fig. 11 - Garnet composition A: T2- (square), T3- (empty circle: Eastern belt; filled circle: Western belt) and T4-amphibolites (triangle). B: gneisses associated with T3.

Garnet

In T3 amphibolites, garnet (Table 7b) shows a wide compositional variability ($\text{Alm}_{49-65}\text{Grs}_{8-27}\text{Prp}_{11-27}\text{Sps}_{1-6}\text{Adr}_{0-9}$), and compositions are homogeneous in samples of comparable bulk composition. They exhibit weak zoning and the pyrope content tends to increase toward the rim. Garnets from one T4 amphibolite differ, due to their high grandite content and low pyrope (Fig. 11A; $\text{Grs}_{37-40}\text{Alm}_{28-36}\text{Adr}_{12-20}\text{Sps}_{4-5}\text{Prp}_{3-4}$), consistent with the low bulk rock $\text{Mg}/\text{Fe}_{\text{tot}}$. In the rodingitized samples the garnet is almost pure grandite ($\text{Grs}_{94-98}\text{Adr}_{0.5-2}\text{Sps}_{0.1-0.2}$), except for one sample with an appreciable Alm (up to 18 mole%). The garnets from the gneisses have a homogeneous almandine composition with significant grandite and pyrope (Fig. 11B; $\text{Prp}_{14-23}\text{Alm}_{63-71}\text{Sps}_{4-8}\text{Grs}_{5-10}$; Table 7c).

Plagioclase

In the T1 amphibolites the An content ranges from 23 to 30 mole%, whereas in T2 the plagioclase is generally saussuritized with rare An_{30} relics. In T3 the composition is in the range An_{31-46} . In T4, plagioclase An_{26-34} sometimes coexists with K-feldspar, mostly pure orthoclase, but compositions with Ab up to 16 mole% as well as Ab exsolutions with K-feldspar ≈ 20 mole% are found. The plagioclase from the gneisses has An_{18-35} .

Micas

The micas from the gneisses and micaschists are biotite and white mica. The biotite from the garnet-bearing gneisses exhibits $\text{TiO}_2 = 1.5-1.7\text{wt}\%$, $\text{Al}_2\text{O}_3 = 18.9-19.9\text{wt}\%$, $\text{Mg}\# \approx 0.6$. The scant biotite from the T4 amphibolite has very low TiO_2 (0.19wt%), $\text{Al}_2\text{O}_3 = 17.54\text{wt}\%$, $\text{Mg}\# \approx 0.70$. The white mica from the garnet-bearing gneisses is muscovite with Fe_2O_3 between 0.6 and 2.4wt%, negligible FeO , and MgO in the range 0.8-1.8wt%. The $\text{Na}/\text{Na}+\text{K}$ is in the range 0.08-0.35 and phengite substitution is negligible.

Accessory phases (ilmenite, epidote)

The ilmenites from the amphibolites are almost pure with appreciable Mn-ilmenite (5-8 mole%) and hematite (3-7 mole%).

The epidotes in equilibrium at the metamorphic peak in the amphibolites are clinozoisites. Their composition depends on the bulk rock composition: low Ps $100*\text{Fe}^{3+}/\text{Fe}^{3+}+\text{Al}^{\text{VI}} = 1.3-1.5$ in T2, and $100*\text{Fe}^{3+}/\text{Fe}^{3+}+\text{Al}^{\text{VI}}$ between 21-26 in T1 and T4. The epidotes included in the garnet of the gneisses have ($100*\text{Fe}^{3+}/\text{Fe}^{3+}+\text{Al}^{\text{VI}} = 16$). The retrograde epidotes tend to near pure Fe-epidote.

Thermobarometric constraints

The Hbl - Plg geothermometer (Blundy and Holland, 1990) was applied to several mineral pairs selected from the different amphibolite types (Table 8). On the whole, the results confirm those in Carosi et al. (1996). For T1, the calibration yields $T = 637 \pm 7^\circ\text{C}$, for P between 0.4-0.5 GPa; T2 gives results of about $624 \pm 9^\circ\text{C}$ for $P \approx 0.5-0.7$ GPa. The Hbl-Plg thermometer for T3 gives the highest values of $755 \pm 33^\circ\text{C}$, for $P \approx 0.7$ GPa. The Grt-Cpx thermometer (Ellis and Green, 1979) applied to T3 yields $T \approx 796 \pm 50^\circ\text{C}$. The Grt - Plg - Hbl - Qtz geobarometer (Kohn and Spear, 1990) applied to the T3 parageneses gives results of about 0.70-0.75 GPa. The Grt-Cpx thermometer calibrations applied to T4 yield $T \approx 755 \pm 55^\circ\text{C}$, for $P \approx 0.7$ GPa. Amphibole-based thermometry could not be applied to T4 due to the sub-silicic composition of the amphibole.

The resulting temperatures are consistent with medium-grade, garnet-free amphibolite facies conditions for T1 and with relatively high T and P, within amphibolite facies at coexisting clinopyroxene and garnet for T3. As for T2, the occurrence of clinopyroxene and the lack of garnet could suggest intermediate conditions between T1 and T3.

However, it should be pointed out that the composition corresponding to cumulus protoliths, characterized by high modal plagioclase and sometimes olivine, with consequent high Mg#, can account for the garnet-free assemblages.

The PT data obtained for T3 and T4 correspond to the suprasolidus conditions of a tholeiitic basalt with $\text{H}_2\text{O} > 5\%$ (Green, 1982). However, geochemical and petrographic evidence of partial melting, except for rare Plg - Qtz veins, is lacking.

We can therefore suppose that the hydrous fluids in equilibrium with the rock could virtually correspond to the amphibole OH-group and, hence, not exceed 2% of the bulk rock composition. Under these PT conditions, the metasediments possibly associated with this origin, could suffer intense partial melting and so be expelled due to differential rheology.

DISCUSSION

The models generally proposed for the obduction of the oceanic lithosphere (e.g., McCaig, 1983; Michard et al., 1991; Cawood and Suhr, 1992; Searle and Cox 1999; Searle et al., 2004 and many others) encompass an early intra-oceanic and a subsequent marginal stage (Michard et al., 1991).

The intra-oceanic stage is characterized by detachment of a section of oceanic lithosphere and subsequent thrusting over a neighbouring one. The detachment level is located within the oceanic mantle, probably along a rheological surface. During the intra-oceanic stage, the metamorphic sole originates in the high-temperature shear zone between the two sections of young and still hot oceanic lithosphere. The metamorphic sole, recognized everywhere at the base of the overriding slice of oceanic lithosphere, is formed by a thick (up to 800 m) assemblage of oceanic-derived rocks, generally deformed and metamorphosed under amphibolite facies conditions. The peridotite overlying the metamorphic sole is affected by mylonitic deformation and serpentinization. The high temperature required for the development of the metamorphic sole is provided by thermal flux from the overthrust mantle tectonites.

In contrast, the marginal stage corresponds to thrusting onto the continental margin of the already cold oceanic lithosphere, in this phase deformed only at its base. Sub-greenschist metamorphism develops in the underlying continental margin sequences. Generally, the marginal stage is characterized by the development of tectonic mélanges and during its latest stage, brittle deformation can dismember the metamorphic sole.

However, some problems are still unresolved in the proposed models (e.g., McCaig, 1981; 1983; Michard et al., 1991; Cawood and Suhr, 1992; Searle and Cox 1999; Searle et al., 2004 and many others), like the geochemical signature of the igneous protoliths, and the occurrence of a veritably inverted metamorphic gradient from amphibolite facies at the top of the metamorphic sole to greenschist facies at its base. In addition, the P and T conditions of the metamorphic climax are still a matter for debate, mainly concerning the pressure attained. The main open question however, regards

the geodynamic setting in which the metamorphic sole originated. Two main environments are proposed in the literature: 1) the metamorphic sole originates during thrusting of a thick section of oceanic lithosphere within a suprasubduction basin, far from a subduction zone (e.g., Michard et al., 1991); 2) the metamorphic sole in the second proposed setting originates in a subduction zone where a slice of hot oceanic lithosphere is underthrust below an accretionary wedge (e.g., Wakabayashi and Dilek, 2003).

The analysis of the metamorphic sole of the Mirdita ophiolites helped to highlight some aspects of the obduction process. The main results are the following:

1. The metamorphic sole consists of an assemblage of slices derived from different protoliths. Different types of amphibolites have been identified, each showing the same

structural history but different P and T values for the climax conditions of their metamorphism. The boundaries between the T1-T4 amphibolite slices as well as those between of gneisses and micaschists are shear zones. This structure pattern and the deformation features can be explained as the result of progressive accretion in a single body - i.e. the metamorphic sole - of slices of different peak metamorphism at different times during the progressive intra-oceanic thrusting of the obducted ophiolites. The slices with the highest metamorphic grade (T3 and T4) were enclosed in the sole shortly after the obduction began, whereas the rocks with the lowest metamorphic grade (T1 and T2) were enclosed subsequently, when the obducting ophiolites were colder. The structure of the metamorphic sole described in this paper is similar to that observed in obducted ophiolites, such

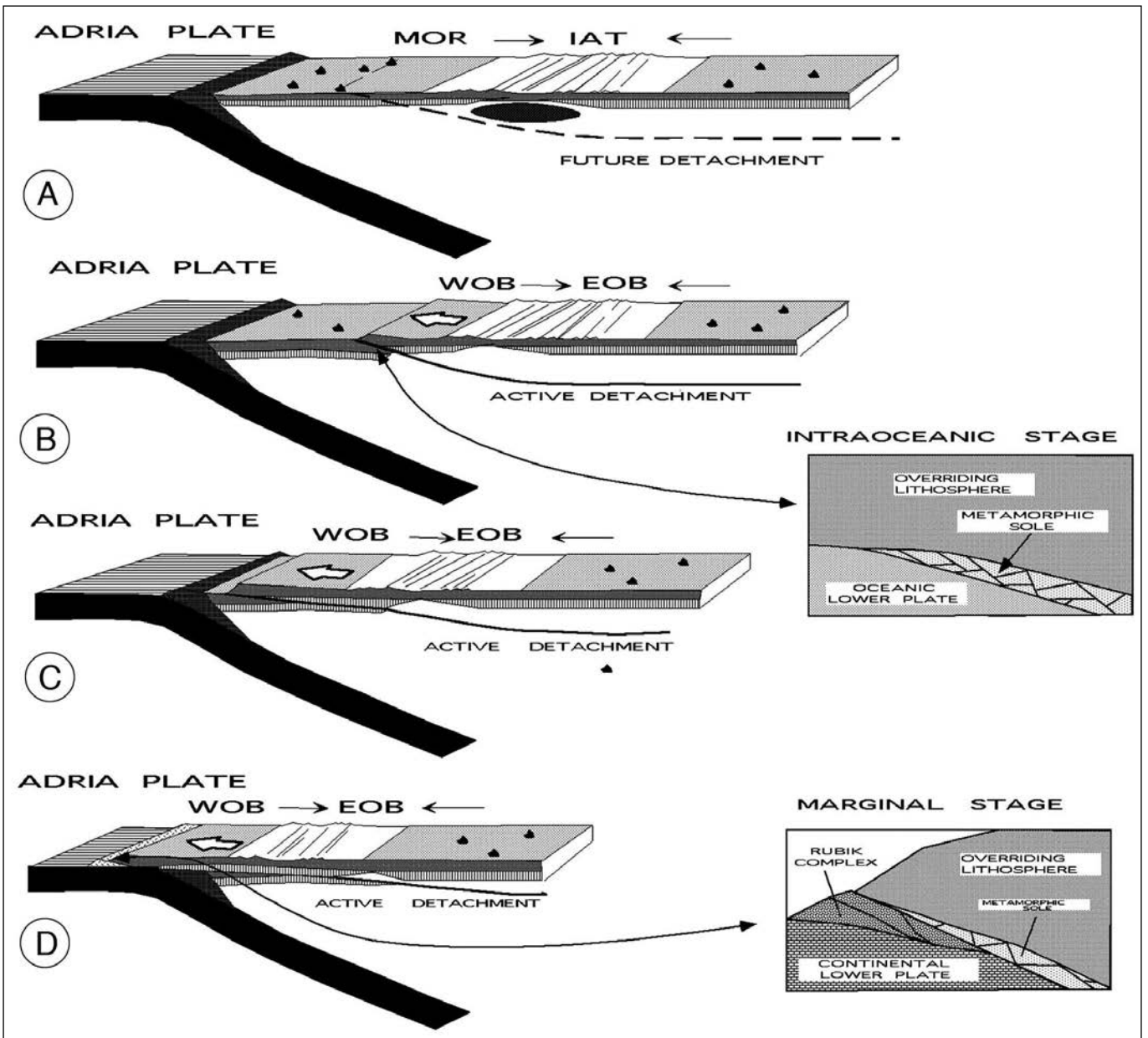


Fig. 12 - Cartoon depicting the dynamics of the Mirdita ocean suture and its obduction. A) subduction and development of a suprasubduction basin with MOR and OIB oceanic lithosphere B) development of an embryonic thrust surface in the suprasubduction basin close to the mid-ocean ridge, along which relatively high temperatures are maintained (e.g. ca 1000°C/km, Boudier et al., 1988). C) Intraoceanic stage of the obduction process. In the enlarged area the relationships between the overriding oceanic lithosphere, the metamorphic sole and the underlying oceanic lower plate are shown D) Marginal stage of the obduction process. In the enlarged area the relationships between the overriding oceanic lithosphere, the metamorphic sole, the Rubik complex and the underlying continental lower plate are shown.

as those in Oman (Hacker and Mosenfelder, 1996).

2. The OIB protoliths of T1, T2 and T3 are defined by their distinctive trace element ratios (Blum et al., 1996) also pointing to a K-alkaline character. Incompatible element abundances normalized to primordial mantle (not reported) match the HIMU-dominated OIBs (Weaver, 1991). Compared with the typical HIMU end-member, the T4 amphibolites show evidence of contamination by crustal-derived material in the sources (Blum et al., 1996) and of partial melting of a mantle source where garnet was a residual phase. The protoliths of the associated paragneisses are probably siliciclastic sediments with subordinate pelite component. Their origin as metarenites/metapelites belonging to an ophiolite sedimentary cover is strongly suggested.

3. The metamorphic overprint in the metamorphic sole is clearly characterized by HT/LP conditions, from lower to higher-grade amphibolite facies. No evidence was found for slices affected only by greenschist metamorphism. The temperature ranged from $624\pm 9^{\circ}\text{C}$ to $796\pm 50^{\circ}\text{C}$ in the slices where pressure was generally lower than 0.7 GPa. These data are consistent with a tectonic load provided by an entire section of oceanic lithosphere ranging in thickness from 15 to 20 km. Pressure values in excess of 1.1 GPa for $T > 750^{\circ}\text{C}$, i.e. largely exceeding our data, were proposed by Dimo-Lahitte et al. (2001). The parameters proposed by Dimo-Lahitte et al. (2001) indicate HP facies conditions, hardly matching the described mineral assemblage represented by diopside and garnet. In addition, the granulites from the Mirdita metamorphic sole are characterized by the occurrence of orthopyroxene (Dimo-Lahitte, 2001), whose absence is diagnostic of HP granulites (e.g., O'Brien and Rotzler, 2003).

4. A discontinuous inverted gradient is observed in the metamorphic sole, where the higher grade amphibolite facies occurs close to the harzburgites. On the whole, the metamorphic sole of the Mirdita ophiolites consists of metamorphic rocks with a decreasing climax metamorphism at increasing structural depth beneath the harzburgites. However, no progressive and continuous change in the P and T conditions of peak metamorphism was observed in the different types of amphibolites.

5. According to e.g., Malpas et al. (1973) and Wakabayashi and Dilek (2003), a rheologically prominent basal horizon is required for a detachment of an entire section of oceanic lithosphere, as the case for the Mirdita ophiolites. Here, the most probable basal detachment horizon is represented by the lithosphere/asthenosphere boundary corresponding to the 1000°C isotherm (Boudier et al., 1988). In addition, a spreading center is generally regarded as the discontinuity where the basal thrust nucleates (e.g., Boudier et al., 1988). Alternatively, emersion of the detachment horizon can be connected with occurrence of a lithospheric discontinuity, possibly represented by a volcanic range, consistent with the large quantity of OIB rocks in this metamorphic sole.

6. A sharp jump in metamorphic characters occurs between the metamorphic sole and the underlying "Volcano-sedimentary Formation", belonging to the Rubik complex, with no evidence of any gradual transition between the two tectonic units. This suggests that the two metamorphic events differ in age and geodynamic significance. The amphibolite facies of the metamorphic sole and its later retrogression to greenschist facies corresponds to the intra-oceanic thrusting phase, whereas the subgreenschist metamorphic overprint can be assumed to have occurred during the subsequent marginal stage.

CONCLUSION

In the Mirdita area, the metamorphic sole consists of an up to 600 m thick assemblage of metasediments and metabasites, mostly amphibolites, at the base of an ophiolitic nappe. Four different amphibolite types were identified for geochemistry, grain-size and mineral assemblages. The protoliths of the amphibolites consist of basic rocks with OIB affinity representative of within-plate magmatism typical of oceanic seamounts. No MORB-derived rocks have been identified. The metasedimentary rocks are in turn likely derived from sedimentary cover of an oceanic crust. All the lithologies from the Mirdita metamorphic sole are strongly deformed under lower to higher amphibolite facies metamorphic conditions. A discontinuous inverted gradient occurs with the rocks showing the highest amphibolite facies metamorphism near the harzburgites. However, no progressive and continuous change in the P and T conditions of the climax metamorphism has been observed in the different types of amphibolites. Greenschist facies metamorphic rocks are absent, although all the lithologies from the Mirdita metamorphic sole are affected by greenschist facies retrogression. The amphibolite types are characterized by different P - T values of metamorphic climax. The temperature ranges from $624\pm 9^{\circ}\text{C}$ to $796\pm 50^{\circ}\text{C}$ in the different types of amphibolites but the pressure is everywhere lower than 0.7 GPa. The boundaries between amphibolite slices with different climax metamorphisms and the bodies of the gneisses and micaschists are shear zones. The structural history, common to all rock types in the Mirdita metamorphic sole, highlights two deformation phases that developed under amphibolite facies metamorphism, followed by a third phase in greenschist facies conditions.

These data fit very well in a model (Figure 12) where the metamorphic sole developed by the intra-oceanic thrusting of a very hot slice of oceanic lithosphere obducted over an adjacent oceanic crust. In this model, progressive thrusting led to formation of the metamorphic sole through the accretion of oceanic seamounts from the lower plate to the base of the overriding plate. The different peak P and T conditions in the amphibolite slices can be interpreted as due to the accretion process through the different stages and to assembly into a single body during the thrusting of the ophiolites (e.g., Hacker and Mosenfelder, 1996). A heat source is required to explain the very high geothermal gradient suggested by the occurrence of amphibolite metamorphism. Residual heat from young, still hot oceanic lithosphere could provide the temperatures required for syn-obduction metamorphism. In addition, frictional heating can be regarded as an additional source during intra-oceanic thrusting. The pressure below 0.7 GPa in all the amphibolite slices is consistent with development of the Mirdita metamorphic sole in a shear zone at the base of an overriding section of oceanic lithosphere not thicker than 15-20 km. Recent models consider obduction process to occur in the lower plate during underthrusting in a flattening subduction zone (e.g., Dimo-Lahitte, 2001). However, the very high geothermal gradient is in contrast with subduction process where metamorphism is characterized by low T/P gradients, and in general by HP conditions. Furthermore, gabbros and basalts from the crustal section lack a HP/LT metamorphic overprint and related pervasive deformation of the whole ophiolite sequence, confirming that the Mirdita ophiolite was not involved in a subduction zone. Moreover, the geochemistry of the Mirdita ophiolites, that points to a suprasubduction origin, as well as the tectono-metamorphic features of the sole, rather suggest that the ob-

duction process was localized in the upper plate, over a subduction zone, where young and still hot oceanic lithosphere was affected by compression immediately after its formation (e.g., Bortolotti et al., 2005). Furthermore, the present data suggest that the entire metamorphic sole developed during an intra-oceanic stage *sensu* Michard et al. (1991), while its emplacement over the continental margin occurred later, when the Mirdita ophiolites were cooled and the metamorphic sole already formed. At this latter stage, only brittle deformation affected the metamorphic sole, as recorded by the brittle faults at its base. Instead, below the overriding obducted oceanic lithosphere, a tectonic mélange, i.e. the Rubik Complex, developed contemporaneously in a brittle regime under sub-greenschist facies metamorphism.

ACKNOWLEDGEMENTS

We would like to dedicate this work Luciano Cortesogno of Genoa University that passed away in May 2005. Luciano Cortesogno started with us this research and contributed a lot in the early phases with his great expertise on ophiolites.

This research was carried out with grants from M.I.U.R. (Project PRIN), C.N.R. (Istituto di Geoscienze e Georisorse) and Genova and Pisa Universities. The authors would like to thank Alaudin Kodra and Farouk Mustafa for fieldwork assistance and stimulating discussions and J. Bébien for his constructive review.

REFERENCES

- Aubouin J., Blanchet R., Cadet P., Celet P., Charvet J., Chorovic J., Cousin M. and Rampoux J.P., 1970. Essai sur la géologie des Dinarides. *Bull. Soc. Géol. France*, 12: 1060-1095.
- Bébien J., Shallo M., Manika K., and Gega D. 1998. The Shebenik Massif (Albania): A link between MOR- and SSZ-type ophiolites?. *Ofioliti* 23:7-15.
- Bébien J., Dimo-Lahitte A., Vergély P., Insergueix-Filippi D., and Dupeyrat L. 2000. Albanian ophiolites. I – Magmatic and metamorphic processes associated with the initiation of a subduction. *Ofioliti* 25:39-45.
- Beccaluva L., Coltorti M., Premti I., Saccani E., Siena F. and Zeda O., 1994. Mid-ocean ridge and supra-subduction affinities in ophiolitic belts from Albania. In: L. Beccaluva (Ed.), *Albanian ophiolites: state of the art and perspective*. *Ofioliti*, 19 (1): 58-77.
- Bellot J.P., Triboulet C., Laverne C. and Bronner G., 2003. Evidence for two burial/exhumation stages during the evolution of the Variscan belt, as exemplified by P-T-t-d paths of metabasites in distinct allochthonous units of the Maures massif (SE France). *Intern. J. Earth Sci.*, 92 (1): 7-26.
- Bhatia M.R. and Crook K.A.W., 1986. Trace element characteristics of graywackes and tectonic discrimination of sedimentary basin. *Contrib. Mineral. Petrol.*, 92: 181-193.
- Blum N., Halbach P. and Munch U., 1996. Geochemistry and mineralogy of alkali basalts from Tropic Seamount, Central Atlantic Ocean. *Marine Geology*, 136: 1-19.
- Blundy J.D. and Holland T.J.B., 1990. Calcic amphibole equilibria and a new amphibole - plagioclase geothermometer. *Contrib. Mineral. Petrol.*, 104: 208-224.
- Bortolotti V., Chiari M., Marcucci M., Marroni M., Pandolfi L., Principi G. and Saccani E., 2004. Comparison among the Albanian and Greek ophiolites, in search of constraints for the evolution of the Mesozoic Tethys ocean. In: L. Beccaluva, V. Bortolotti, M. Marroni, L. Pandolfi, G.B. Piccardo, E. Saccani and R. Tribuzio (Eds.), *Italian researches on Mediterranean ophiolites: selected contributions*. *Spec. Issue, Ofioliti*, 29: 19-35.
- Bortolotti V., Chiari M., Kodra A., Marcucci M., Marroni M., Mustafa F., Pandolfi L., Prella M., Principi G. and Saccani E. 2006. Triassic MORB magmatism in the Southern Mirdita zone (Albania). *Ofioliti*, 31: 1-9.
- Bortolotti V., Kodra A., Marroni M., Mustafa F., Pandolfi L., Principi G. and Saccani E., 1996. Geology and petrology of ophiolitic sequences in the Mirdita region (northern Albania). *Ofioliti*, 21 (1): 3-20.
- Bortolotti V., Marroni M., Pandolfi L. and Principi G., 2005. Mesozoic to Tertiary tectonic history of the Mirdita ophiolites, northern Albania. *The Island Arc*, 14 (4): 471-493.
- Bortolotti V., Marroni M., Pandolfi L., Principi G. and Saccani E., 2002. Alternation of MOR and SSZ basalts in Albanian ophiolites: Evidences of interactions between Mid-Ocean Ridge and subduction-related processes in an infant arc setting. *J. Geol.*, 110: 561-576.
- Boudier F., Ceuleneer G. and Nicolas A. 1988. Shear zones, thrusts and related magmatism in the Oman ophiolite: initiation of thrusting on an oceanic ridge. *Tectonophysics*, 151: 275-296.
- Carosi R., Cortesogno L., Gaggero L. and Marroni M. 1996. Geological and petrological features of the metamorphic sole from the Mirdita nappe, northern Albania. *Ofioliti*, 21 (1): 21-40.
- Cawood P.A. and Suhr G. 1992. Generation and obduction of ophiolites; constraints for the Bay of Islands Complex, western Newfoundland. *Tectonics*, 11: 884-897.
- Chiari M., Bortolotti V., Marcucci M. and Principi G. 2008. New data on the age of Simoni Mélange, Northern Mirdita Ophiolite Nappe, Albania. *Ofioliti*, 32: 53-56.
- Cloos M. and Shreve R.L. 1988. Subduction-channel model of prism accretion, mélange formation, sediment subduction, and subduction erosion at convergent plate margins: 2. Implications and discussion. *Pure Appl. Geophys. (Historical Archive)*, 128 (3-4): 501-545.
- Coleman R.G. 1981. Tectonic setting for ophiolite obduction in Oman. *J. Geophys. Res.*, 86 (B4): 2497-2508.
- Çollaku A., Cadet J.P., Bonneau M. and Jolivet L., 1992. L'édifice structural de l'Albanie septentrionale: des éléments de réponse sur les modalités de la mise en place des ophiolites. *Bull. Soc. Géol. France*, 163 (4): 455-468.
- Çollaku A., Cadet J.P., Bonneau M. and Kienast J.R., 1991. La semelle métamorphique infra-ophiolitique de la nappe de la Mirdita, son métamorphisme inverse et ses relations avec la série volcano-sédimentaire (région de Lura, Albanie septentrionale). *C. R. Acad. Sci. Paris*, 313 (2): 251-258.
- Cortesogno L., Gaggero L., Jaho E., Marroni M., Pandolfi L. and Shtjefanaku D., 1998. The gabbroic complex of the western ophiolitic belt, Northern Albania: an example of multilayered sequence in an intermediate-spreading oceanic ridge. *Ofioliti*, 23 (2): 49-64.
- Dilek Y., Furnes H. and Shallo M. 2007. Suprasubduction zone ophiolite formation along the periphery of Mesozoic Gondwana. *Gondwana Res.*, 11 (4): 453-475.
- Dilek Y., Furnes H. and Shallo M. 2008. Geochemistry of the Jurassic Mirdita Ophiolite (Albania) and the MORB to SSZ evolution of a marginal basin oceanic crust. *Lithos* 100 (1-4): 174-209.
- Dilek Y., Shallo M. and Furnes H., 2005. Rift-drift, seafloor spreading, and subduction tectonics of Albanian ophiolites. *Intern. Geol. Rev.*, 47 (2): 147-176.
- Dimo-Lahitte A., Monié P. and Vergély P., 2001. Metamorphic soles from the Albanian ophiolites: Petrology, ⁴⁰Ar/³⁹Ar geochronology, and geodynamic evolution. *Tectonics*, 20 (1): 78-96.
- Ellis D.J. and Green E.H., 1979. An experimental study of the effect of Ca upon garnet-clinopyroxene Fe-Mg exchange equilibria. *Contrib. Mineral. Petrol.*, 71: 13-22.
- Fleet M.E. and Barnett R.L., 1978. Al^{IV}/Al^{VI} partitioning in calciferous amphiboles from the Froid mine, Sudbury, Ontario. *Can. Mineral.*, 16: 527-532.
- Gawlick H.J., Frisch W., Hoxha L., Dumitrica P., Krystyn L., Lein R., Missoni S. and Schlagintweit F., 2008. Mirdita Zone ophi-

- lites and associated sediments in Albania reveal Neotethys Ocean origin. *Intern. J. Earth Sci.*, 97 (4): 865-881.
- Gray D.R. and Gregory R.T., 2000. Implications of the structure of the Wadi Tayin metamorphic sole, the Ibra-Dasir block of the Samail ophiolite, and the Saih Hatat window for late stage extensional ophiolite emplacement, Oman. *Marine Geophys. Res.*, 21 (3-4): 211-227.
- Green T.H., 1982. Anatexis of mafic crust and high pressure crystallization of andesite. In: R.S. Thorpe (Ed.), *Andesites*. Wiley, New York, p. 465-487.
- Gromet L.P., Dymek R.F., Haskin L.A. and Korotev R.L., 1984. The North American shale composite: Its compilation, major and trace element characteristics. *Geochim. Cosmochim. Acta*, 48: 2469-2482.
- Hacker B.R. and Mosenfelder J.L., 1996. Metamorphism and deformation along the emplacement thrust of the Samail ophiolite, Oman. *Earth Planet. Sci. Lett.*, 155: 435-451.
- Hawthorne F.C. and Oberti R., 2007. Classification of the amphiboles. *Reviews in Mineralogy & Geochemistry*. Mineral. Soc. Am., Geochem. Soc., Accad. Naz. Lincei, 67: 55-88
- Hoek V., Koller F., Meisel T., Onuzi K. and Kneringer E., 2002. The Jurassic South Albanian ophiolites: MOR- vs. SSZ-type ophiolites. *Lithos*, 65 (1): 143-164.
- Hoxha M. and Boullier A.M., 1995. The peridotites of Kukes ophiolite (Albania): structure and kinematics. *Tectonophysics*, 249: 217-231.
- Hoxha M., Boullier A.M. and Zhupi S., 1993. Structure des peridotites de l'ophiolite de Kukes (Albanie). *Bull. Soc. Géol. France*, 164 (3): 449-458.
- Kodra A., Gjata K. and Xhomo A., 2000. Tectonic history of Mirdita oceanic basin. *Bul. Shkencave Gjeol.*, Tirana, 1: 5-26.
- Insergueix-Filippi D., Dupeyrat L., Dimo-Lahitte A., Vergely P. and Bébien, J. 2000. Albanian ophiolites. II - Model of subduction zone infancy at a Mid-ocean ridge. *Ofioliti* 25:47-53.
- Kohn M.J. and Spear F.S., 1990. Two new barometers for garnet amphibolites with applications to eastern Vermont. *Am. Mineral.*, 75: 89-96.
- Kretz R., 1983. Symbols for rock-forming minerals. *Am. Mineral.*, 68: 277-279.
- Kurz W. and Froitzheim N., 2002. The exhumation of eclogite facies metamorphic rocks - a review of model confronted with examples from the Alps. *Intern. Geol. Rev.*, 44 (8/1): 702- 743.
- Laird J. and Albee A.L. 1981. Pressure, temperature, and time indicators in mafic schists: their application to reconstructing the polymetamorphic history of Vermont. *Am. J. Sci.*, 281: 127-175.
- Leake B.E., Woolley A.R., Arps C.E.S., Birch W.D., Gilbert M.C., Grice J.D., Hawthorne F.C., Kato A., Kisch H.J., Krivovichev V.G., Linthout K., Laird J., Mandarino J.A., Maresch W.V., Nickel E.H., Rock N.M.S., Schumacher J.C., Smith D.C., Stephenson N.C.N., Ungaretti L., Whittaker E.J.W. and Youzhi G., 1997. Nomenclature of amphiboles: report of the subcommittee on amphiboles of the International Mineralogical Association, Commission on new minerals and mineral names. *Can. Mineral.*, 35: 219-246
- Leake B.E., Woolley A.R., Birch W.D., Burke E.A.J., Ferraris G., Grice J.D., Hawthorne F.C., Kisch H.J., Krivovichev V.G., Schumacher J.C., Stephenson N.C.N. and Whittaker E.J.W. 2003. Nomenclature of amphiboles: additions and revisions to the International Mineralogical Association's 1997 recommendations. *Can. Mineral.*, 41: 1355-1362
- Lytwyn J.N. and Casey J.F., 1995. The geochemistry of postkinematic mafic dike swarms and subophiolitic metabasites, Pozanti-Karsanti Ophiolite, Turkey; evidence for ridge subduction. *Geol. Soc. Am. Bull.*, 107 (7): 830-850.
- Malpas J., Stevens R. and Strong D.F., 1973. Amphibolite associated with Newfoundland and ophiolite: its classification and tectonic significance. *Geology*, 1 (1): 45-47.
- Marcucci M. and Praela M., 1996. The Lumi i zi (Puke) section of the Kalur Cherts: radiolarian assemblages and comparison with other sections in northern Albania. *Ofioliti*, 21 (1): 71-76.
- McCaig A.M., 1983. P-T conditions during emplacement of the Bay of Islands Ophiolite Complex. *Earth Planet. Sci. Lett.*, 63: 459-473.
- Meneghini F., Marroni M., Moore J.C., Pandolfi L., Rowe C.D. 2009. The process of underplating in the geologic record: structural diversity between the Franciscan Complex (California), the Kodiak Complex (Alaska) and the Internal Ligurian Units (Italy). *Geol. J.*, 44 (2): 126-152.
- Meschede M., 1986. A method of discriminating between different types of mid-ocean ridge basalts and continental tholeiites with the Nb-Zr-Y diagram. *Chem. Geol.*, 56: 207-218.
- Michard A., Chopin C. and Goffé B., 1991. Obduction versus subduction and collision in the Oman case and in the other Tethyan setting. In: T.J. Peters, A. Nicolas and R.G. Coleman (Eds.), *Ophiolite genesis and evolution of the oceanic lithosphere. Petrology and structural geology*. Kluwer Acad. Publ., London, 5: 447-467.
- Miller J.A. and Cartwright I., 2000. Distinguishing between seafloor alteration and fluid flow during subduction using stable isotope geochemistry: examples from Tethyan ophiolites in the Western Alps. *J. Metam. Geol.*, 18 (5): 467-482.
- Morimoto N., Fabries J., Ferguson A.K., Ginzburg I.V., Ross M., Seifert F.A., Zussman J., Aoki K. and Gottardi G., 1988. Nomenclature of pyroxenes. *Am. Mineral.*, 73: 1123-1133.
- Nakamura N., 1974. Determination of REE, BA, Fe, Mg, Na and K in carbonaceous and ordinary chondrites. *Geochim. Cosmochim. Acta*, 38: 757-775.
- Nicolas A., Boudier F. and Meshi A., 1999. Slow spreading accretion and mantle denudation in the Mirdita ophiolite (Albania). *J. Geophys. Res.*, 104 (B7), 15: 155-15,167.
- O'Brien P.J. and Rotzler J., 2003. High-pressure granulites: formation, recovery of peak conditions and implications for tectonics. *J. Metam. Geol.*, 21: 3-20.
- Pearce J.A. and Parkinson I.J., 1993. Trace element models for mantle melting: application to volcanic arc petrogenesis. In: H.M. Prichard, T. Alabaster, N.B.W. Harris and C.R. Neary (Eds.), *Magmatic processes and plate tectonics*. Geol. Soc. London Spec. Publ., 76: 373-403.
- Robertson A.H.F. and Dixon J.E., 1984. Introduction: aspects of the geological evolution of the Eastern Mediterranean. In: J.E. Dixon and A.H.F. Robertson (Eds.), *The geological evolution of the Eastern Mediterranean*. Geol. Soc. London Spec. Publ., 17: 1-73.
- Robertson A.H.F. and Shallo M., 2000. Mesozoic-Tertiary tectonic evolution of Albania in its regional eastern Mediterranean context. *Tectonophysics* 316: 197-254.
- Rock N.M.S., 1990. The International Mineralogical Association (IMA/CNMMN) Pyroxene nomenclature scheme: Computerization and its consequences. *Mineral. Petrogr.*, 43: 211-227.
- Roser B.P. and Korsch R.J., 1988. Provenance signature of sandstone - mudstone suites determined using function analysis of major element data. *Chem. Geol.*, 67: 119-139.
- Saccani E., Beccaluva L., Coltorti M. and Siena F., 2004. Petrogenesis and tectonomagmatic significance of the Albanide - Hellenide Subpelagonian ophiolites. *Ofioliti* 29 (1): 75- 93.
- Saccani E., Bortolotti V., Marroni M, Pandolfi L. and Photiades A., 2008b. The Jurassic association of backarc basin ophiolites and calc-alkaline volcanics in the Guevgueli Complex (Northern Greece): implication for the evolution of the Vardar Zone. *Ofioliti*, 33 (2): 209-227.
- Saccani E., Photiades A., Santato A. and Zeda O., 2008a. New evidence for supra-subduction zone ophiolites in the Vardar zone of Northern Greece: implications for the tectono-magmatic evolution of the Vardar Oceanic basin. *Ofioliti*, 33(1): 65-85
- Searle M. and Cox J., 1999. Tectonic setting, origin and obduction of the Oman ophiolite. *Geol. Soc. Am. Bull.*, 111: 104-122.
- Searle M.P., Warren C.J., Waters D.J. and Parrish R.R., 2004. Structural evolution, metamorphism and restoration of the Arabian continental margin, Saih Hatat region, Oman mountains. *J. Struct. Geol.*, 26: 451-473.
- Shallo M., 1994. Outline of the Albanian ophiolites. In: L. Becca-

- luva (Ed.), Albanian ophiolites: state of the art and perspectives. Spec. Issue, *Ofioliti*, 19 (1): 57-75.
- Shallo M., Kote D. and Vranai A., 1987. Geochemistry of the volcanics from ophiolitic belts of Albanides. *Ofioliti*, 12: 125-136.
- Spray J.G., 1983. Lithosphere-asthenosphere decoupling at spreading centers and initiation of obduction. *Nature*, 304: 253-255.
- Stampfli G.M., Mosar J., Marquer D., Marchant R., Baudin T. and Borel G., 1988. Subduction and obduction processes in the Swiss Alps. *Tectonophysics*, 296: 159-204.
- Vergely P., Dimo A. and Monié P., 1998. Datation des semelles métamorphiques ophiolitiques d'Albanie par la méthode $^{40}\text{Ar}/^{39}\text{Ar}$: conséquences sur le mécanisme d'obduction. *C. R. Acad. Sci. Paris*, 326: 717-722.
- Wakabayashi J. and Dilek Y., 2003. What constitutes "emplacement" of an ophiolite?: Mechanisms and relationship to subduction initiation and formation of metamorphic soles. In: Y. Dilek and Robinson P.T. (Eds), *Ophiolites and Earth history*. Geol. Soc. London Spec. Publ., 218: 427-448.
- Weaver B.L., 1991. The origin of oceanic island basalt end-member compositions: trace element and isotopic constraints. *Earth Planet. Sci. Lett.*, 104: 381-397.
- Wenjiao X., Brianf W., Jie H. and Jiliang L., 2002. Arc-ophiolite obduction in the Western Kunlun Range (China): implications for the Palaeozoic evolution of central Asia. *J. Geol. Soc.*, 159 (5): 517-528.
- Winchester J.A. and Floyd P.A., 1977. Geochemical discrimination of different magma series and their differentiation products using immobile elements. *Chem. Geol.*, 20: 325-343.
- Wood D.A., Tarney J. and Weaver B.L., 1981. Trace element variations in Atlantic ocean basalts and Proterozoic dykes from North-west Scotland: their bearing upon the nature and geochemical evolution of the upper mantle. *Tectonophysics*, 75: 91-112.

Received, December 20, 2008

Accepted, June 4, 2009